

Use of flow visualization data to examine spatial–temporal velocity and burst-type characteristics in a turbulent boundary layer

By L. J. LU AND C. R. SMITH

Department of Mechanical Engineering and Mechanics, Lehigh University, Bethlehem,
PA 18015, USA

(Received 5 March 1990 and in revised form 26 April 1991)

It is well known that turbulence production in turbulent boundary layers occurs in short, energetic bursts; however, the relationship between the results of pointwise burst detection techniques and the spatial flow structure associated with such burst-type events has not been clearly established. To address this point, a study using VITA detection of burst-type events was done which allows the direct comparison between flow visualization results and quantitative, temporal velocity profile data for a flat-plate turbulent boundary layer. Using automated image processing of hydrogen-bubble flow visualization pictures, temporal velocity profile data are established using a corrected time-of-flight technique for velocity extraction. Using the visualization-derived data, spatial-temporal velocity-derived properties ($\partial u/\partial y$, $\partial u/\partial t$, etc.), as well as probe-type burst detection properties are established. In addition, temporal and ensemble-averaged burst-type characteristics are shown to be essentially identical to previous VITA-detected velocity probe results. The VITA approach is extended to establish the spatial extent of burst-type events and the ensemble-averaged spatial-temporal properties associated with VITA-based detection. By use of a regionalized detection procedure, the types of burst-type patterns are categorized and compared with the associated visualization sequences.

1. Introduction

Since the benchmark studies at Stanford and Ohio State Universities (Kline *et al.* 1967; Corino & Brodkey 1969; Kim, Kline & Reynolds 1971; and Nychas, Hershey & Brodkey 1973) it has been well known that turbulence production in turbulent boundary layers is a quasi-periodic process which results in short, energetic production of turbulent energy termed ‘bursting’. Since a detailed understanding of the bursting process holds the potential for improving both dynamic modelling of the turbulence production cycle and methods for control of surface drag and heat transfer, much attention has been focused on the turbulent bursting process.

The seminal studies of bursting cited above relied heavily on flow visualization, and were the first to recognize the presence and significance of quasi-deterministic and quasi-periodic coherent structures in a turbulent boundary layer. The classic study of Kline *et al.* (1967) established the presence of a quasi-coherent process of turbulence generation which was termed the ‘bursting’ process. This process was described as the wall migration of low-speed fluid, a gradual ‘lift-up’ and subsequent oscillation of this low-speed fluid (termed a ‘streak’), followed by the sudden break-up and ejection of the low-speed from the surface. They speculated that this

'bursting' event dominates the momentum and energy transfer between the inner and outer regions of turbulent boundary layers. This speculation was later sustained by Kim *et al.* (1971), who demonstrated that the main turbulence production process adjacent to a solid surface is indeed due to the short, quasi-periodic production of turbulent energy during the bursting process.

Using a combination of tracer particles and a moving stereoscopic camera system, Corino & Brodkey (1969) observed a sequence of coherent events, consisting of the ejection of fluid from local regions of decelerated fluid, which occurred in conjunction with a high-speed sweep motion, with this process repeating randomly in space and time (i.e. a quasi-deterministic process). Similar behaviour was also observed and described in broader scope in a subsequent study of coherent structures in a turbulent boundary layer by Nychas *et al.* (1973).

In an attempt to quantify the characteristics of the turbulent bursting process, several techniques have been developed which attempt to detect bursting behaviour by the evaluation of velocity signals from one or more velocity probes. (See Luchik & Tiederman 1987 and Tiederman 1989 for an overview of these techniques.) One of the earliest and most utilized techniques is the VITA (i.e. variable-interval time average or short-time variance) technique developed by Blackwelder & Kaplan (1976) (for a detailed formulation see §3.4). Basically, this technique is a method for detecting 'bursting' or regions of high activity in a probe signal by examination of the variance over a short time sample (e.g. $5 < T^+ < 25$, where $T^+ = Tu_r^2/\nu$). Employing the VITA technique, Blackwelder & Kaplan determined typical bursting frequencies of $f^+ = 0.0041$ at $y^+ = 15$ (where $f^+ = f\nu/u_r^2$, and $y^+ = u_r/\nu$). Expanding the use of the VITA detection technique, Blackwelder & Haritonidis (1983) further investigated the scaling of the bursting frequency in turbulent boundary layers. Their results suggest that (i) the bursting frequency appears to scale on inner variables (shear velocity, u_r , and kinematic velocity, ν) rather than on outer variables (free-stream velocity, U_∞ , and boundary-layer thickness, δ), and (ii) the sensor size is an important parameter, which must be less than $20\nu/u_r$ in length to avoid spatial-averaging effects and assure consistent results.

Johansson & Alfredsson (1982) and Alfredsson & Johansson (1984) used conditional averaging from the VITA detection technique to account for both accelerating and decelerating bursting events. Employing the positive and negative slope of the u -signal as their reference, they made a detailed examination of the positive, negative, and total bursting frequencies as a function of the VITA detection threshold (k) and the VITA averaging time interval (T). Their results show that the VITA technique singles out events of a duration which is roughly equal to the averaging time used in the detection criterion.

The comparison of observed flow-visualized bursting to probe-detected bursting was first done by Offen & Kline (1974) using dye-slot flow visualization and hot-film measurements. Their results were inconclusive, since visually observed 'bursts' often had no coincidence with the probe detections. The general examination of combined dye-probe results was later extended at Purdue University (Bogard & Tiederman 1986; Luchik & Tiederman 1987; Tiederman 1989), where it was established that adequate coincidence between dye-marked and probe-detected bursting requires a significant streamwise distance for dye migration before the dye will properly mark a burst-type event, and that burst-type events may consist of more than one 'ejection' (a point first made by Corino & Brodkey 1969). It was further established that, when properly employed, the most common probe burst detection schemes (quadrant two, u -level, modified u -level, and VITA techniques) all seem to yield the

same average time between bursts, or events of high activity, although all the single-point detection techniques only capture a portion of the total burst-type event, usually some portion of a single ejection.

One of the difficulties in performing burst detections is that the processes which occur in a turbulent boundary layer appear to occur over a region and a broad range of scales. Recent work using numerical simulations (Kim, Moin & Moser 1987; Robinson, Kline & Spalart 1989) underscores this point. Robinson, in particular, demonstrates that the flow structures and events occurring in a turbulent boundary layer appear in a variety of repetitive forms, but at varying scales and levels of activity. Robinson's work suggests that turbulence-producing events are both temporally and spatially distributed, and generally associated with the presence of vortical structures of one form or another. Robinson tends to move away from the characterization of bursting as a singular type of event to the characterization and taxonomy of the types of detected events related to turbulence production. However, it is important to establish that the characteristics demonstrated by simulations also occur in the experimental environment, and there are still serious questions as to the relationship between the results of broadly utilized burst detection schemes and the classic, visually-identified burst sequence of Kim *et al.* (1971). In general, little progress has been made in establishing 'regionalized' approaches for experimental detection of a flow structure or in providing direct methods of correlation between visual and probe data. As pointed out above, Tiederman and his colleagues have compared dye-probe results, but a direct correlation in which the cross-stream velocity field was monitored has not been done experimentally. As Tiederman (1989) points out, 'Hydrogen bubble flow visualization from a wire normal to the wall is the preferred method for detecting bursts, because all bursts immediately downstream of the normal wire will be marked'. One approach which will allow the combined evaluation of hydrogen-bubble visualization and velocity information is to use image processing of hydrogen-bubble pictures to quantitatively establish instantaneous cross-stream velocity data.

Manual techniques for quantifying hydrogen-bubble flow visualization have been previously employed by Kim *et al.* (1971) for one-dimensional, streamwise measurement. Manual measurements in two dimensions have been done using segmented bubble wires by Grass (1971) in a vertical plane and by Kasagi, Hirata & Nishino (1986) in a spanwise plane. Note that the difficulties with the two-dimensional techniques arise from the technical problems encountered in segmentally insulating a hydrogen bubble wire to allow the generation of squares of marker bubbles, and in compensating for the wake effect created by the insulated segments. Three-dimensional manual processing has been used by Smith & Paxson (1983) for reconstructed time-line display. A semi-automated processing technique was attempted by Cornelius, Takenchi & Deutsch (1977) for one-dimensional, streamwise measurement; more recently, Lu & Smith (1985), developed a similar semi-automated technique which allowed acquisition of an extensive data set sufficient for determination of one-dimensional turbulence statistics.

Note that the above quantitative visualization studies pay only limited attention to burst-type behaviour, and none address regional burst-type detection and comparison; the present investigation addresses this deficiency by considering both regional detection and one-to-one comparison of spatial velocity-visualization data. The present paper is an extension of the work of Lu & Smith (1985), illustrating techniques for acquiring turbulent boundary layer space-time velocity data with hydrogen-bubble wires, and providing a detailed comparison of spatial VITA-

detected burst-type events with the actual visualization sequences, including a categorization of the type and scales of detected events.

2. Test system and data acquisition

2.1. Test facility and conditions

The flow facility used in the present study is a free-surface, Plexiglas water channel of dimensions $5 \times 0.9 \times 0.36$ m. The details of the facility are described by Metzler (1980) and Cerra & Smith (1983). The test surface was a 2.5 m Plexiglas flat plate, 6.35 mm thick with a 6:1 half-ellipse leading edge, located 10 cm above the channel floor; the mean flow velocity was held at 18.3 cm/s. To assure a consistent transition location, a trip constructed of 5 rows of staged polystyrene beads (2 to 3 mm in diameter) was located 5 cm from the leading edge (see Johansen & Smith 1983, for details and verification). The resulting turbulent boundary layer properties at a test location 1.8 m from the leading edge were established experimentally as $Re_\theta = 1120$ (where $\theta =$ momentum thickness) and $u_r = 0.786$ cm/s, with a free-stream turbulence intensity of 0.3%.

2.2. Hydrogen-bubble technique

In the present study, flow visualization was done using the hydrogen-bubble method as described by Clutter, Smith & Brazier (1961) and Schraub *et al.* (1965). A 20 μ m diameter platinum wire was oriented normal to the plate, passing through a 0.5 mm hole in the plate which was sealed on the opposing side. The other end of the bubble wire was soldered to a coiled copper wire which acted as both a conductor for the bubble-wire circuit and as a tensioning agent to keep the bubble wire taut (see figure 1). This arrangement allowed visualization of the entire boundary layer all the way to the surface of the plate. The platinum wire served as the cathode in the bubble-wire circuit; a 6 mm diameter graphite rod, located downstream of the bubble wire, served as the anode. The bubbles generated by the wire are of the order of one-half the wire diameter, which renders buoyancy effects negligible over the region of interest (Schraub *et al.* 1965). The frequency of bubble-line generation is phase-locked to the framing rate of the video viewing system using a specially designed bubble-pulse generator and synchronization circuit. An electrolyte of sodium sulphate (0.15 g Na_2SO_3 /l of water) was added to the water channel to enhance bubble generation. This results in the production of denser bubble lines, which provide better clarity and contrast for the visual data.

2.3. Video system

The hydrogen-bubble time lines were viewed and recorded using an INSTAR high-speed video system manufactured by the Video Logic Corporation. The video system incorporates synchronized strobe lights to provide 120 frames/s, with an effective shutter speed of 10 μ s. This short exposure time effectively freezes the bubble-line pattern such that high-contrast sequences of discrete pictures may be obtained.

In the present study, the video camera was mounted as shown in figure 1, providing side views of the vertical hydrogen-bubble wire. The output from the camera can be viewed on-line with a high-resolution TV monitor and simultaneously recorded on one-inch video tape. Visualization sequences may be replayed in real-time, flicker-free slow motion (forward or reverse), or in sequential, single-frame stop-action for detailed data analysis.

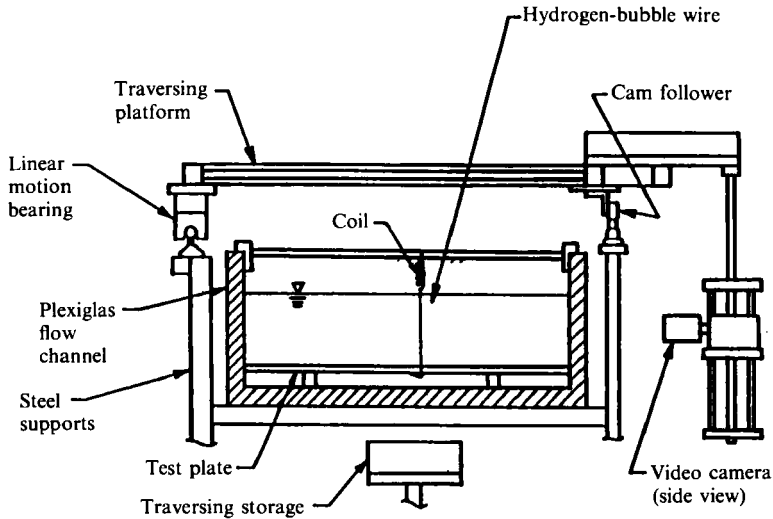


FIGURE 1. End-view schematic of flow channel and viewing technique (from upstream).

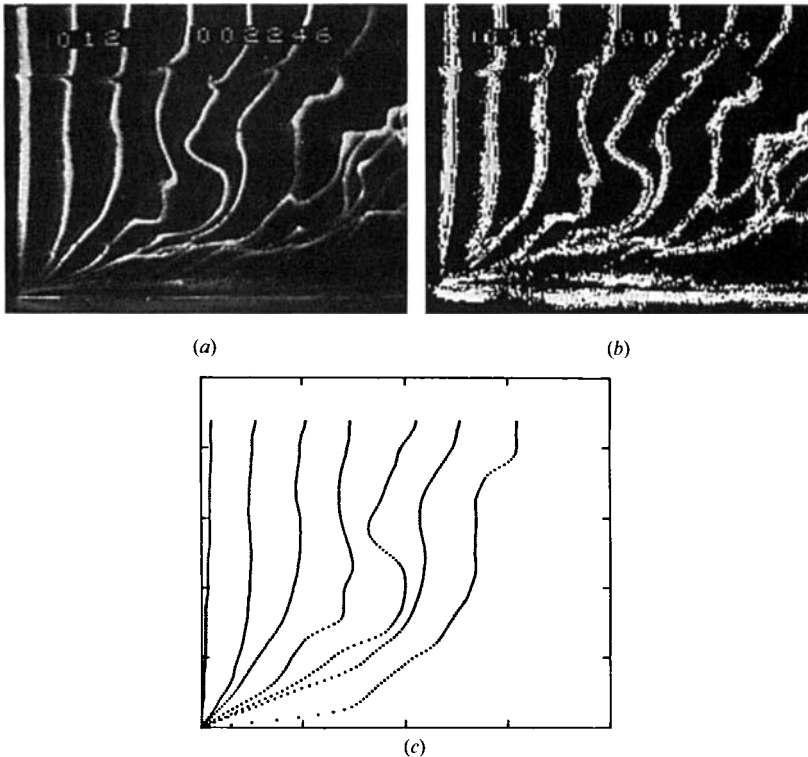


FIGURE 2. Computer-identified hydrogen-bubble lines. (a) Original frame from video sequence, (b) computer-enhanced picture, (c) plot of identified bubble lines (Lu & Smith 1985).

2.4. Image-processing technique

To determine quantitative velocity profile data from the hydrogen-bubble-line patterns, individual video frames are converted to a 512×512 digital array with a range of 256 grey levels using a GOULD IP8500 image-processing system interfaced with a DEC Micro VAX II computer. To allow quantitative evaluation of the time-

line patterns, each individual digital array is recalled and scanned to establish the location of the first three bubble timelines. To locate each bubble line in the image, the digital images are first digitally filtered and digitally differentiated with respect to the horizontal (x) direction, yielding an 'image' of the x -direction gradient of the original image; the leading edge of each bubble line is established from this gradient image by locating the adjoining points along the maximum negative x -direction gradient. The result of this procedure is a two-dimensional array representing the computer-identified locations of the time lines (see Lu & Smith 1985 for the details of the procedure). Figure 2 shows computer-identified hydrogen-bubble lines for a scene from the present study.

3. Data reduction

3.1. Velocity determination

For each bubble-line picture, the profiles of instantaneous horizontal velocity are established using time-of-flight techniques as outlined in Schraub *et al.* (1965) and Lu & Smith (1985). The local bubble-line velocity at each point is approximated as $U_b = \Delta x / \Delta t$, where Δx is the horizontal displacement between the two bubble time-lines nearest the generating wire, and Δt is the time-line generation period.

The bubbles generated in the wake of a hydrogen-bubble wire move slightly slower than the local fluid velocity owing to the wake defect of the wire (see Davis & Fox 1966; Grass 1971; and Abernathy, Bertschy & Chin 1977). The bubble velocity can be compensated for by considering the wake defect behind a circular cylinder (see, for example, Schlichting 1979). This effect can be generally represented by a simplified form of the full laminar wake equation as

$$\frac{(U_{\text{act}} - U_{\text{bub}})}{U_{\text{act}}} = C \left(\frac{\Delta x}{d} \right)^{-n},$$

where Δx is the streamwise distance of hydrogen bubbles from the generating wire, d the diameter of hydrogen bubble-wire, U_{bub} the bubble velocity (i.e. $U_{\text{bub}} = \Delta x / \Delta t$), U_{act} the true fluid velocity, and C , n are empirical constants. Bubble velocity data taken in the present flow facility using a bubble wire towed at constant speeds through the quiescent channel indicates that $C = 1.7$ and $n = 0.5$ provide a reasonable fit of the velocity data, which is consistent with the results of Abernathy *et al.* (1977). Using the above equation, the bubble-line velocity data were computer-corrected to yield the local fluid velocity over the bubble-pulse period.

Note that the corrected velocity is not a true instantaneous value since it entails essentially a Taylor approximation (i.e. that the corrected Lagrangian time-line velocity reflects the local Eulerian velocity). However, this assumption is reasonable because of the limited transit distance between bubble time lines and the relatively short averaging time ($\Delta t^+ = \Delta t u_0^2 / \nu = 2$).

The accuracy of the above assumption is illustrated by Lu & Smith (1985), where they demonstrate a close comparison between turbulent boundary-layer velocity statistics determined using the present image-processing approach and accepted probe-measured statistics (see also Lu & Smith 1988; Smith & Lu 1989).

3.2. Velocity fit near the wall

Note that very near the wall ($y^+ < 4$ to 5), reflected light from the wall makes it very difficult to discriminate the bubble-line location; in addition, the low relative velocity within this region requires excessive defect correction. In the study of Lu &

Smith (1985) linear behaviour was assumed from the velocity determined at $y^+ \approx 5$ down to the zero-slip condition at the wall. However, it is well known that the instantaneous streamwise pressure gradient beneath a flat-plate turbulent boundary layer ($\partial p/\partial x$) varies in time, although the mean pressure gradient must average zero. Evaluating the Navier–Stokes equation at the wall ($y = 0$) indicates that the instantaneous pressure gradient is directly related to the second derivative of instantaneous streamwise velocity normal to the wall (i.e. $(1/\rho) (\partial p/\partial x) = \nu(\partial^2 u/\partial y^2)$ at $y = 0$). Thus, by the above reasoning, $(\partial^2 u/\partial y^2)_{y=0}$ must be able to take instantaneous non-zero values. It is also expected that $(\partial p/\partial x)$ will also experience instantaneous variations normal to the surface.

These above two criteria suggest that the simplest minimum function which should fit the time-dependent velocity behaviour in the wall sublayer is a third-order polynomial of the form $u^+(t, y^+) = a(t)y^{+3} + b(t)y^{+2} + c(t)y^+ + d(t)$, where $u^+ = u/u_\tau$. Thus, for each measured velocity profile in the present study, the constants for the polynomial were determined using the last three measured points and the assumption of zero velocity at the wall. Employing this fitting procedure to establish the time-dependent profiles within the sublayer region, and then time-averaging over the entire turbulence sequence yields a time-mean sublayer profile of the form $\bar{u}^+(y^+) = \bar{a}y^{+3} + \bar{b}y^{+2} + \bar{c}y^+$, with the coefficient values for the present turbulence data determined as $\bar{a} = -0.00174$, $\bar{b} = -0.0015$ and $\bar{c} = 1.005$. At the wall, the mean velocity profile must satisfy the wall compatibility conditions which are

$$\frac{\partial \bar{u}^+}{\partial y^+} = 1, \quad \frac{\partial^2 \bar{u}^+}{\partial y^{+2}} = \frac{\partial \bar{p}^+}{\partial x^+}, \quad \frac{\partial^3 \bar{u}^+}{\partial y^{+3}} = 0 \quad \text{at } y^+ = 0.$$

The present results give

$$\frac{\partial \bar{u}^+}{\partial y^+} = \bar{c} = 1.005, \quad \frac{\partial^2 \bar{u}^+}{\partial y^{+2}} = 2\bar{b} = -0.003, \quad \frac{\partial^3 \bar{u}^+}{\partial y^{+3}} = 6\bar{a} = -0.01 \quad \text{at } y^+ = 0.$$

The above results are quite close to the required wall compatibility conditions, suggesting the viability of the fitting process. Note that the 0.5% deviation in $\partial \bar{u}^+/\partial y^+$ and the minimal deviation in $\partial^3 \bar{u}^+/\partial y^3$ can be attributed to accumulated uncertainty due to differentiation of the data. The same uncertainty applies to $\partial^2 \bar{u}^+/\partial y^2$ also, but the small negative variation does appear reasonable when compared to the mean pressure gradient approximated from changes in the mean flow external to the boundary layer. Note that the mean pressure gradient in the free stream can be expressed as

$$\overline{\partial p/\partial x} = -\rho U_\infty(x) dU_\infty(x)/dx,$$

which can be non-dimensionalized as

$$(1/\mu)(\overline{\partial p/\partial x})^+ = -U_\infty(x)[dU_\infty(x)/dx][\nu/u_\tau^3].$$

For the present case, this non-dimensional pressure gradient is approximated using velocity measurements within the free stream to be $[(1/\mu)\overline{\partial p/\partial x}]^+ \approx -0.0035$ (a slightly favourable pressure gradient due to displacement of the free stream by the developing boundary layer), which is essentially the same as the value determined by differentiation of the velocity profile curve fit.

Differentiation of the mean velocity profile obtained by the third-order curve fit yields a value of $u_\tau = 0.786$ cm/s. This is 5% lower than the value of $u_\tau = 0.823$ cm/s

that is obtained by a fit of the velocity data to the logarithmic, law-of-the-wall region [$u^+ = 2.44 \ln(y^+) + 4.9$]. The trend of these results is consistent with previous results for probe measurements of low-Reynolds-number turbulent boundary layers by Kline *et al.* (1967) and Purtell, Klebanoff & Buckley (1981).

3.3 Velocity-derivative properties

Employing the sequential velocity profile data ($u(t, y)$), derivative properties of $\partial u/\partial y$, $\partial^2 u/\partial y^2$, and $\partial u/\partial t$ were determined numerically using spline fits with continuous second derivatives, from which local derivatives in either space ($\partial u/\partial y$ and $\partial^2 u/\partial y^2$) or time ($\partial u/\partial t$) were established. In the region $0 < y^+ < 5$, the first and second derivatives with y are evaluated from the cubic polynomial curve fits as described previously.

3.4 VITA technique

The VITA (variable-interval time-average or short-time variance) technique developed by Blackwelder & Kaplan (1976) is often employed for detecting ‘bursting’ (construed as local regions of high activity) in a probe signal by examination of the local variance over a limited time window. The VITA parameter is evaluated from the fluctuating velocity data using the standard relationship:

$$\text{VITA} = \frac{\text{Var}(t, T)}{u_{\text{rms}}} = \frac{\frac{1}{T} \int_{t-T/2}^{t+T/2} u'(s)^2 ds - \left[\frac{1}{T} \int_{t-T/2}^{t+T/2} u'(s) ds \right]^2}{u_{\text{rms}}}$$

where u' is the fluctuating velocity, u_{rms} the turbulence intensity, T the short-time averaging interval and t time.

The VITA variance reflects the local excursion of a time-dependent signal from the local mean. As such, the VITA parameter is indicative of local ‘activity’ about the local mean value, with a turbulent burst *assumed* to be reflective of a region of high local activity. By specifying an arbitrary threshold level (e.g. $\text{VITA} = k = 1$), the VITA parameter is employed as a quantitative indication of the occurrence of a ‘burst’ (Blackwelder & Haritonidis 1983). Note that the VITA parameter is strongly dependent on the value of the averaging time window, T , which acts as a filter on the basic velocity data.

3.5 Profile filter via orthogonal decomposition

Because of noise introduced into the profiles due to image-processing uncertainty (a detailed uncertainty discussion is given in Lu 1985), the proper orthogonal decomposition method as described by Lumley (1967) is applied to the present profile data as a low-pass spatial filter (see Lu & Smith 1988, 1991 for details). Basically, the instantaneous velocity profiles of the turbulent boundary layer are decomposed into a set of eigenfunctions ($\psi_i^{(n)}$) and their corresponding eigenvalues ($\lambda^{(n)}$) which are used to evaluate the corresponding eigenmodes (i.e. $\lambda^{(n)} \psi_i^{(n)}(y) \psi_j^{(n)}(y)$). Note that the sum of the eigenmodes corresponds to the stress tensor, $T_{ij}(y) = \sum_n \lambda^{(n)} \psi_i^{(n)}(y) \psi_j^{(n)}(y)$ (where i, j indicate the streamwise and normal directions); in the present study, ψ represents the eigenfunction for the streamwise component of velocity only. Since the sum of the eigenvalues reflects the total energy of the flow field, using orthogonal decomposition as a velocity profile filter allows the deletion of the lower-energy, higher-frequency, small-scale modes, while retaining the higher-energy, lower-frequency modes which represent the more dominant flow structure.

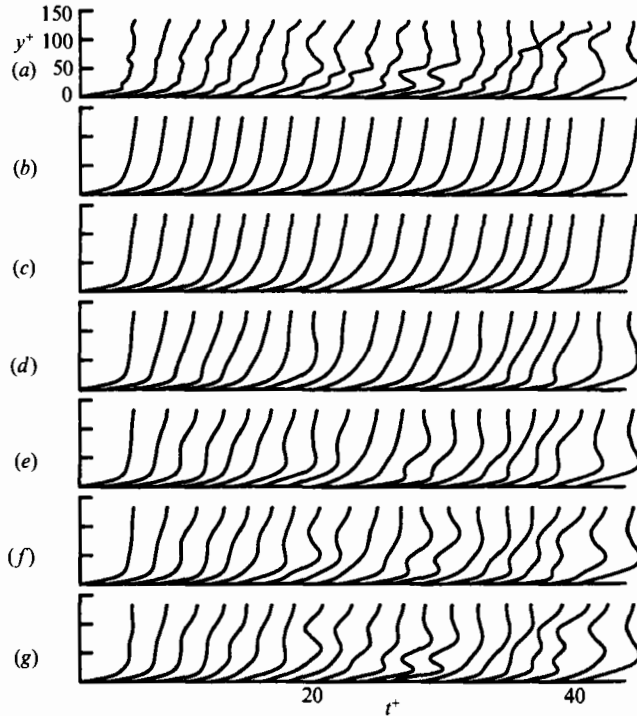


FIGURE 3. (a) Original temporal velocity profiles and the reconstructed profiles obtained by summation up to (b) the 1st, (c) 2nd, (d) 3rd, (e) 4th, (f) 5th, and (g) 6th local eigenmodes, as determined from orthogonal decomposition

$$\left(u_{(N)}(t, y) = \sum_{n=1}^N a^{(n)}(t) \psi^{(n)}(y), \quad N = 1, \dots, 6 \right).$$

The recovery of temporal velocity profiles by the cumulative summation of the local eigenmodes is shown in figure 3. The original velocity profile is shown, followed by profiles reconstructed by sequential summation of progressively higher-order eigenmodes. Note that recovery of the original temporal velocity profiles requires the summation of eigenmodes of higher order than are required for recovery of the time-mean velocity profile (see Lu & Smith 1988, 1991). For the present results, we have employed temporal velocity profiles that are reconstructed using the first six eigenfunctions obtained from decomposition of the total velocity; this reconstruction process recovers over 99.9% of the kinetic energy of the original temporal velocity profiles.

4. Velocity statistics and characteristics

4.1. Statistical results

In figure 4, mean velocity, turbulence intensity, skewness and flatness obtained from the reconstructed velocity profiles are shown in comparison with data obtained using the original velocity profiles. Figure 4 indicates that the mean velocity and all higher-moment profiles are essentially identical for both the original velocity data and the reconstructed velocity data, with the exception of the skewness ($\overline{u^3}/u_{\text{rms}}^3$) and flatness ($\overline{u^4}/u_{\text{rms}}^4$) in the region $y^+ < 9$. This departure very near the surface for the

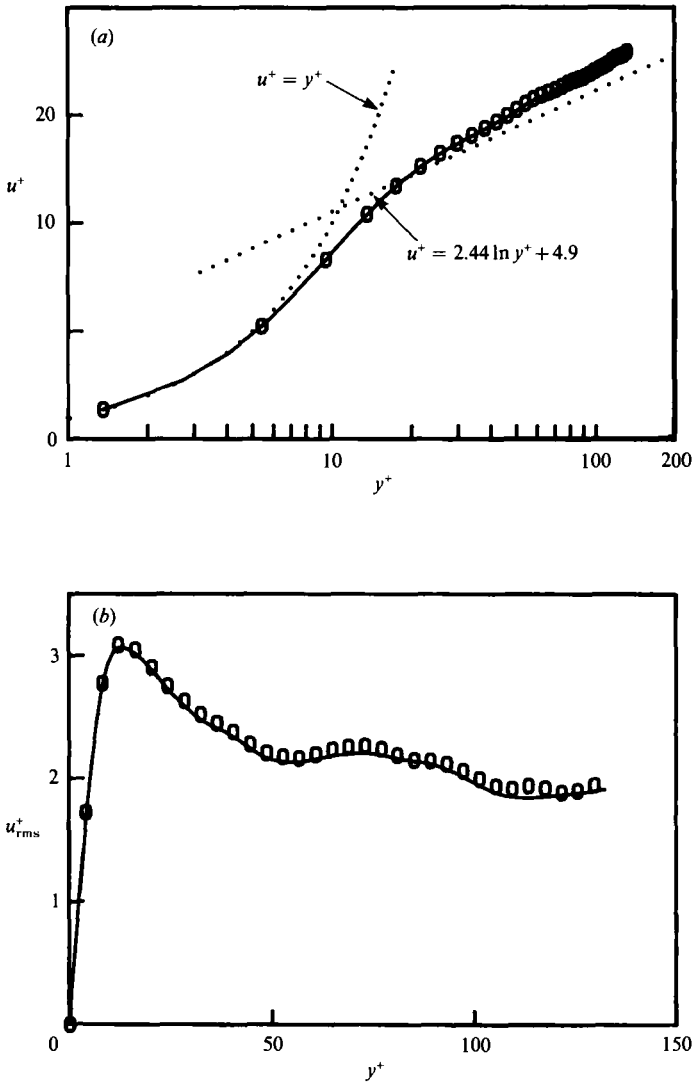


FIGURE 4(a, b). For caption see facing page.

higher-moment statistics is apparently due to the loss of higher-frequency, small-scale information by the decomposition process. The corresponding power spectrum results, determined from the reconstructed velocity data at selected heights, are shown in figure 5. Again, these results conform to conventional turbulent-boundary-layer power spectrum decay characteristics. In addition, a detailed evaluation of profiles of mean and fluctuating derivative values of $\partial u/\partial y$ and $\partial^2 u/\partial y^2$ has been done, and can be found in Lu & Smith (1988).

4.2. Illustration of local, time-dependent characteristics

Reconstructed velocity profiles and the corresponding velocity-derived property profiles covering a time segment of $\Delta t^+ = 40$ (out of a total sequence record of $\Delta t^+ = 2024$) are shown in figure 6(b)–(h); a selected set of visualization frames from the original video sequence are shown in figure 6(a). Examples of the derived velocity

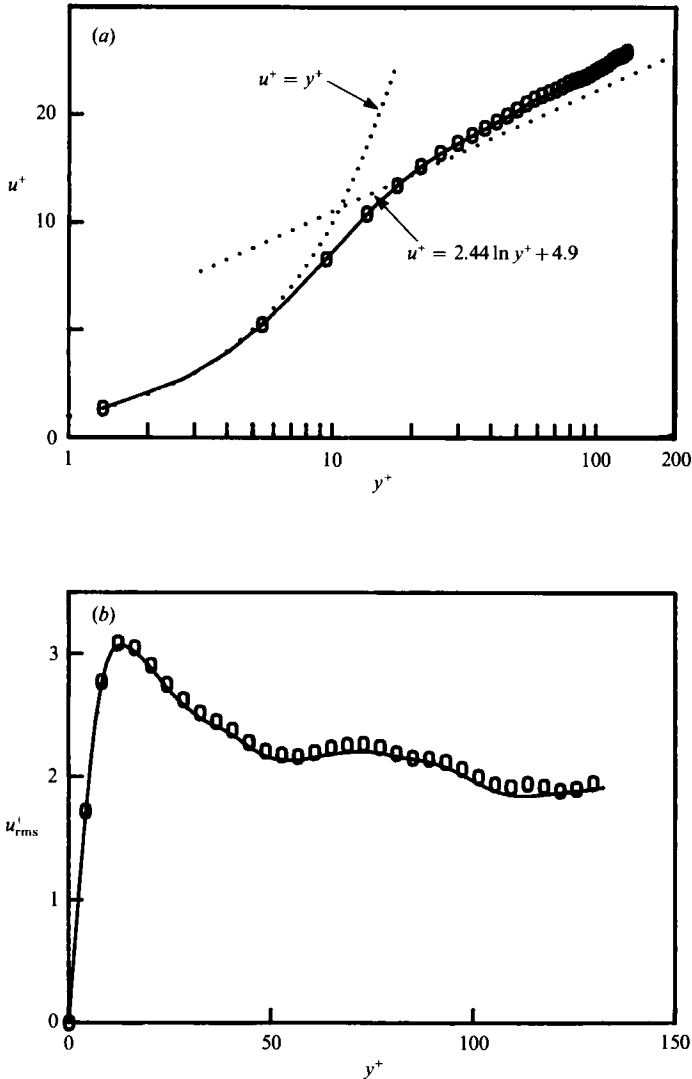


FIGURE 4. Comparison of reconstructed velocity statistics with original data: o, original turbulence data; — full velocity decomposition result. (a) Mean velocity profile (semi-log), (b) turbulence intensity, (c) skewness, (d) flatness.

profiles (u) and velocity fluctuation ($u' = u - \bar{u}$) are shown in figures 6(b) and 6(c). As illustrated in Lu & Smith (1985, 1988), time-averaged statistics obtained from the image-processed velocity profiles are essentially the same as previous probe-measured data for mean velocity, turbulence intensity, skewness and flatness. Using these velocity profiles, the resulting short-time variance parameter employed in the probe-based VITA burst detection technique of Blackwelder & Kaplan (1976) was established (using a $T^+ = 10$ averaging window). A segment of the corresponding VITA profiles appears in figure 6(g).

To expand beyond the conventional velocity, velocity fluctuation, and VITA data, the velocity profile data were differentiated using numerical spine fits (see §3.3) to establish the velocity properties of $\partial u / \partial y$, $\partial^2 u / \partial y^2$, and $\partial u / \partial t$. The respective profiles are shown in figures 6(d), 6(e) and 6(f). It has been suggested and demonstrated by

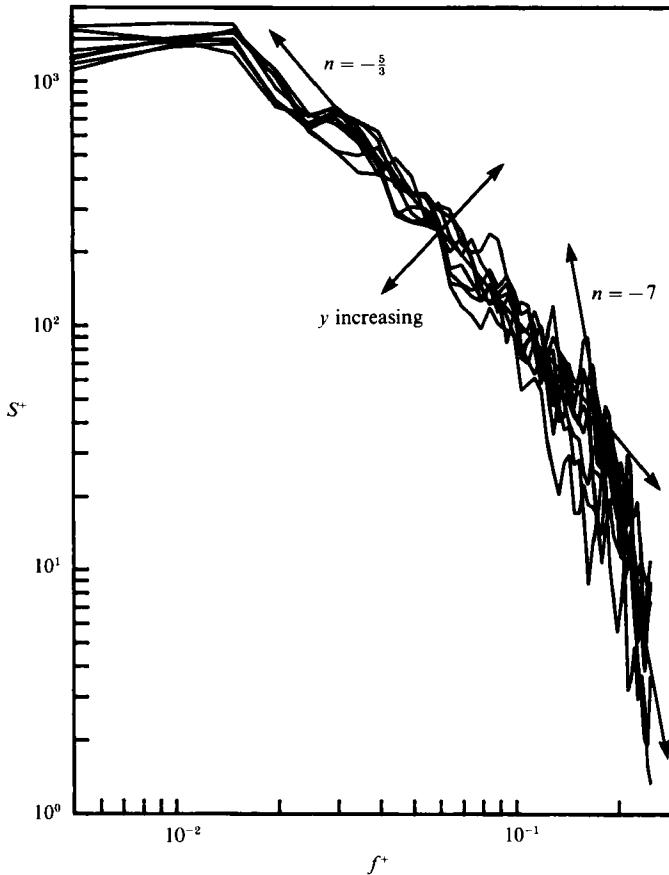


FIGURE 5. Power spectrum results at selected heights ($0 < y^+ < 140$) for full velocity decomposition case:

$$\delta^+(f^+) = \int_{-\infty}^{\infty} R_{ij}(\tau^+) e^{-2\pi i f^+ \tau^+} d\tau^+, \text{ where } f^+ = f\nu/u_\tau^2.$$

White (1974), Eckelmann *et al.* (1977), and Kim (1983) that $\partial u/\partial y$ is, in general, the most significant contribution to the spanwise vorticity. In addition, the local properties of $\partial u/\partial y$ and $\partial^2 u/\partial y^2$ at the wall ($y = 0$) are also respectively proportional to the instantaneous wall shear stress and the fluctuating pressure gradient (see §3.2).

Because VITA and local acceleration ($\partial u/\partial t$) are often employed as indicators of local turbulent burst-type behaviour, the convolution of these two properties ($\text{VITA} \times \partial u/\partial t$) can be employed to discriminate between the 'accelerating' and 'decelerating' bursts of Johansson & Alfredsson (1982). An example of profiles of this latter property is shown in figure 6(h), providing a clear indication of the level and direction of change within regions of local burst-like activity.

The display of flow property profiles, such as shown in figure 6, is one technique for display of general flow property behaviour and for comparison of velocity data with the observed flow visualization patterns. An alternative presentation technique is the use of isocontour plots of cross-stream flow property behaviour. This has particularly nice applications for the study of the time-dependent characteristics of a turbulent boundary layer since the closed contours illustrate 'regions' of local

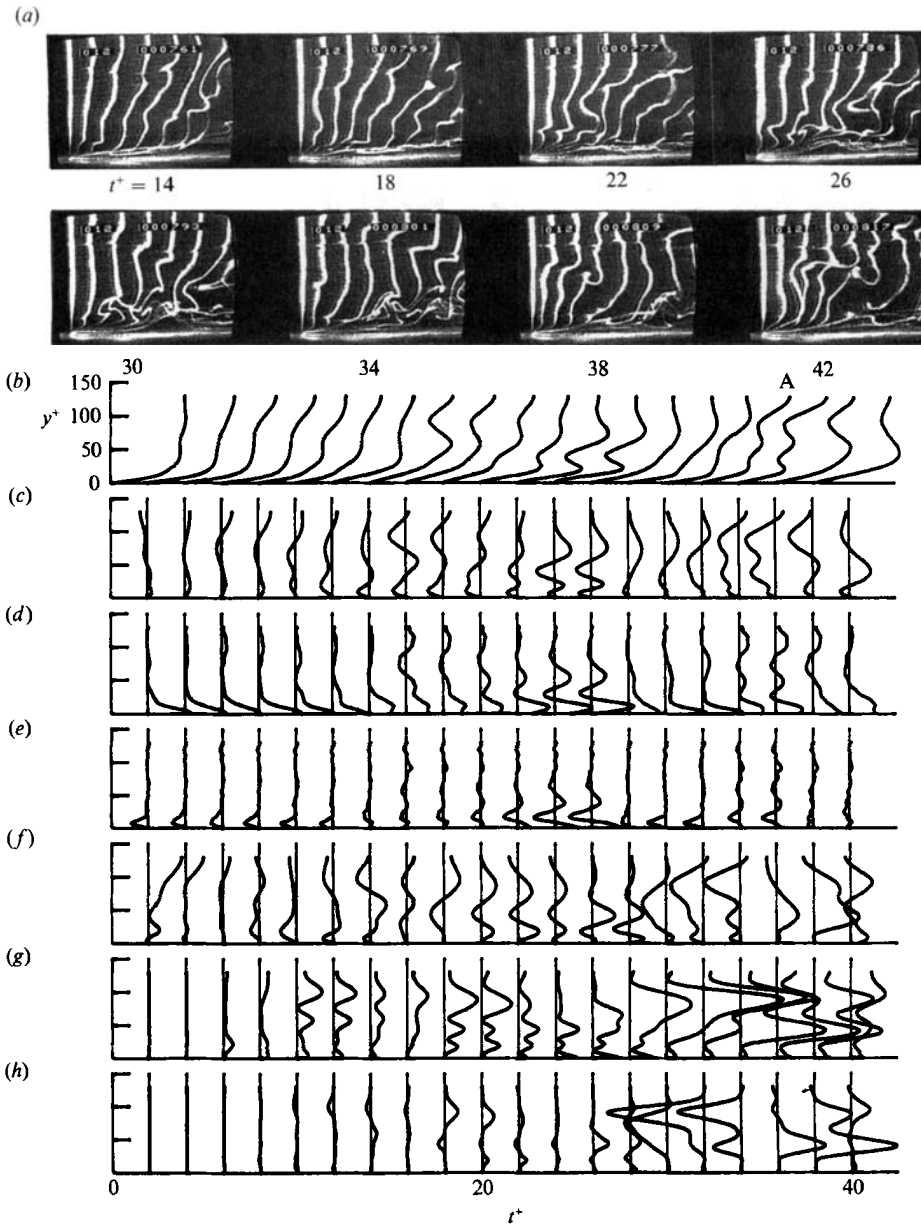


FIGURE 6. Comparison of (a) visual sequence with (b)–(h) profiles of velocity and velocity-derived properties obtained from turbulent-boundary-layer sequence, $0 < t^+ < 40$. (b) u (profile interval $\Delta u^+ = 8$), (c) u ($\Delta u^+ = 8$), (d) du/dy ($\Delta du^+/dy^+ = 1$), (e) d^2u/dy^2 ($\Delta d^2u^+/dy^{+2} = 0.2$), (f) du/dt ($\Delta du^+/dt^+ = 2$), (g) VITA ($\Delta VITA = 1$), (h) VITA $\times du/dt$ ($\Delta(VITA \times du^+/dt^+) = 0.4$).

property variation. Figure 7 is an isocontour presentation of the same data as shown in figure 6. As is illustrated in the VITA profiles and contours of figures 6 and 7, burst-type events appear quite localized and unlikely to be universally detected by a single-sensor measurement of the velocity signal at a fixed location (note that $15 \leq y^+ \leq 30$ is the characteristic measurement region employed for probe ‘detection’ of turbulent bursts). Clearly, the detection of burst-type activity would appear to be most properly done and characterized on a ‘regionalized’ basis. Using the present

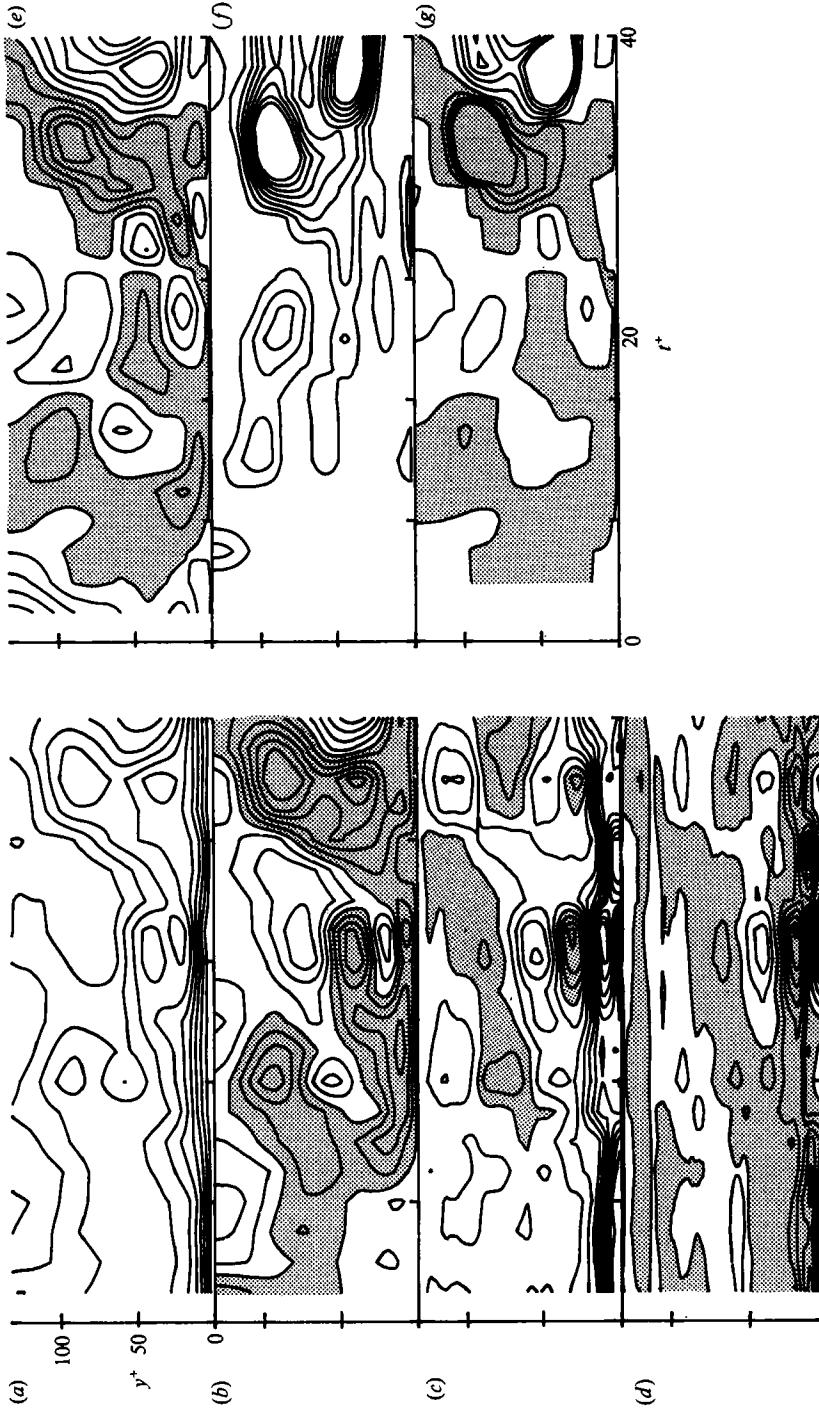


FIGURE 7. Contour plots of velocity and velocity-derived properties corresponding to temporal profiles in figure 6. (a) u (contour interval $\Delta u^* = 2$), (b) $u' (\Delta u^* = 1)$, (c) $du/dy (\Delta du^*/dy^* = 0.1)$, (d) $d^2u/dy^2 (\Delta d^2u^*/dy^{*2} = 0.1)$, (e) $du/dt (\Delta du^*/dt^* = 0.02)$, (f) VITA $(\Delta VITA = 0.25)$, (g) VITA $\times du/dt (\Delta VITA \times du^*/dt^* = 0.4)$. Shaded regions indicate negative values.

data, VITA-detected events are examined and characterized using two different approaches: (i) by establishment of conditional ensemble averages of flow property space-time patterns based on local detection of both accelerating and decelerating events, and (ii) by the identification and classification of typical burst-type space-time characteristics (i.e. velocity, velocity-derived properties, and visual sequences) based on regionalized VITA detection.

5. Examination of burst-type events

5.1. Conditional sampling

Utilizing the present space-time data, the VITA property was used to construct ensemble averages of the flow property profile behaviour in the vicinity of detected events. Employing an averaging window of $T^+ = 10$ and using $k = 1$ as a criterion for a detected event, the flow profile properties in the vicinity $-10 \leq t^+ \leq 10$ were ensemble averaged for all detected burst-type events in the sequence. Since there is some growing disagreement as to what the appropriate definition of a burst is, we use the term 'burst' loosely to mean the regions of high activity detected by the prescription of a particular VITA threshold, and shall refer to these interchangeably as both 'bursts' and detected or burst-type events, with the former reflective of past common usage and the former the more conservative description of these detections. Figure 8 shows ensemble-averaged streamwise velocity traces at selected heights above the surface for burst-type detections at points where $y^+ = 15, 30, 65,$ and 100 . Figure 8 is similar to the mode of presentation usually employed with probe rakes (e.g. Blackwelder & Kaplan 1976, and Hogenes & Hanratty 1982), with the patterns in this figure appearing essentially identical to the probe rake results of Blackwelder & Kaplan (1976) (cf. their figure 12 with figure 8 at $y^+ = 15$). Figure 8 indicates that in the vicinity of the detection location the velocity patterns are identical to those detected with single probes (e.g. Blackwelder & Kaplan 1976; Johansson & Alfredsson 1982), with the characteristic pattern diminishing with distance from the detection point. Note that the degree of diminution occurs most rapidly for detection points near the wall, suggesting that the extent of a detected event is generally smaller within this region.

The respective ensemble averages for both accelerating and decelerating events centred at $y^+ = 15, 30,$ and 65 are shown in isocontour form in figure 9. In these isocontour plots, closed VITA contours circumscribe the detection location, with the central VITA value in excess of unity except for the case where $y^+ = 30$. Note that because all of the velocity-derived properties shown in figure 9 are developed from the ensemble-averaged velocity profiles shown in these figures, this yields an 'averaged' set of flow characteristics, which have been effectively filtered by the ensemble averaging process. This averaging process reduces local magnitudes and gradients, and loses much of the information on smaller-scale structure. Thus, the 'averaged' VITA values in figure 9 may be much less than the individual event contributions. Note that if the average values of all the original local peak VITA values at each detection point are computed, the 'average' VITA values at $y^+ = 15, 30,$ and 65 are approximately 1.3, 1.2, and 1.5 respectively, which are all in excess of unity, as they must be.

Note that a peak VITA contour reflects a region of either acceleration or deceleration (as demonstrated by the $VITA \times \partial u / \partial t$ contour plots), and also reflects an interface between negative and positive velocity excursions (see the u' contour plots). Note also how, for all three figures, the velocity isocontours are characterized

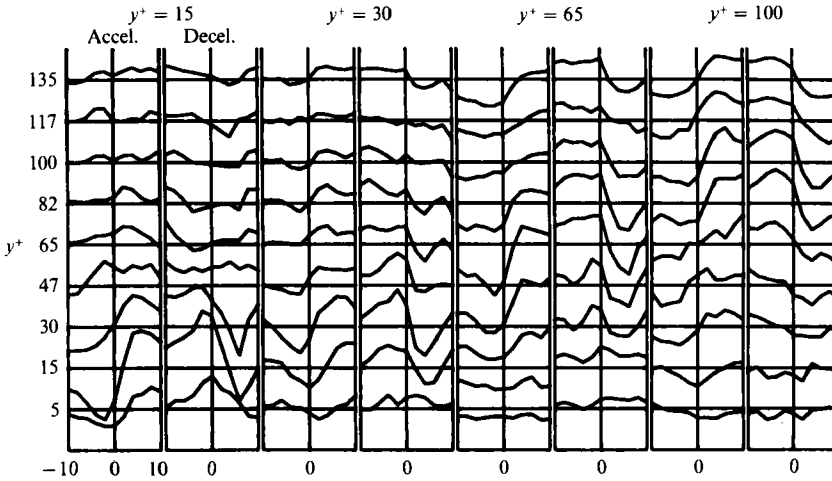


FIGURE 8. Conditional ensemble-averaged results of streamwise velocity behaviour at selected heights above surface for $y^+ = 15, 30, 65$ and 100 detection points; accelerating and decelerating detections ($\Delta u^+ = 4$).

by descending or ascending ‘humps’ in the u contours, with a descending hump corresponding to an accelerated-VITA event, and an ascending hump reflecting a decelerated-VITA event. The types of physical processes giving rise to these patterns are discussed further in §5.3. Note, however, that the accelerated-VITA events, which are much more common than decelerated events, are quite similar to the events described in the vanguard visualization studies by Kline *et al.* (1967), Corino & Brodkey (1969), Kim *et al.* (1971), Nychas *et al.* (1973), and Offen & Kline (1975), who suggest that as fluid is ejected outward during a burst event, it is followed almost immediately by a higher-speed flow which ‘sweeps’ down toward the surface.

The isocontour plots of u' , $\partial u/\partial y$, and to some degree, $\partial^2 u/\partial y^2$ also display characteristic patterns for the burst-type behaviour. The general characteristics are most clearly exemplified in the left portion of figure 9*a*, which shows the conditional behaviour for VITA detection with $k = 1$ and $\partial u/\partial t > 0$ at $y^+ = 15$, the most commonly employed location and criteria for single-probe detection. The characteristic burst-type pattern for u' displays a systematic negative/positive variation, with an interface (or shear layer) inclined to the surface by between 10° and 20° ; this interface angle becomes steeper as the detection point is moved outward. Note that this pattern is essentially identical (if one performs a time–space transformation of the abscissa in figure 9) to similarly derived ensemble-averaged figures shown in Johansson, Alfredsson & Kim (1989) (their figure 4, from probe measurements, and figure 5*b*, from numerical simulations), wherein VITA-detection criteria identical to the present study were employed. In the general vicinity of the u' interface, the velocity gradient, $\partial u/\partial y$, is observed to develop a positive focus just above the detection location; this bears a strong similarity (again performing a time–space transformation) to instantaneous strong shear-layer characteristics observed in numerical simulations (Jimenez *et al.* 1988; Moser 1989; and Robinson *et al.* 1989), which also appear to be initiated at shallow angles to the surface, and become more pronounced with increased distance from the surface. As illustrated by the contours of $\partial^2 u/\partial y^2$, this focus is inflexional ($\partial^2 u/\partial y^2 \approx 0$), suggesting the presence of an instability in the velocity gradient. This inflexional behaviour is clearly observed in figure 10, where the data of figure 9(*a*) are plotted in conventional profile form, and

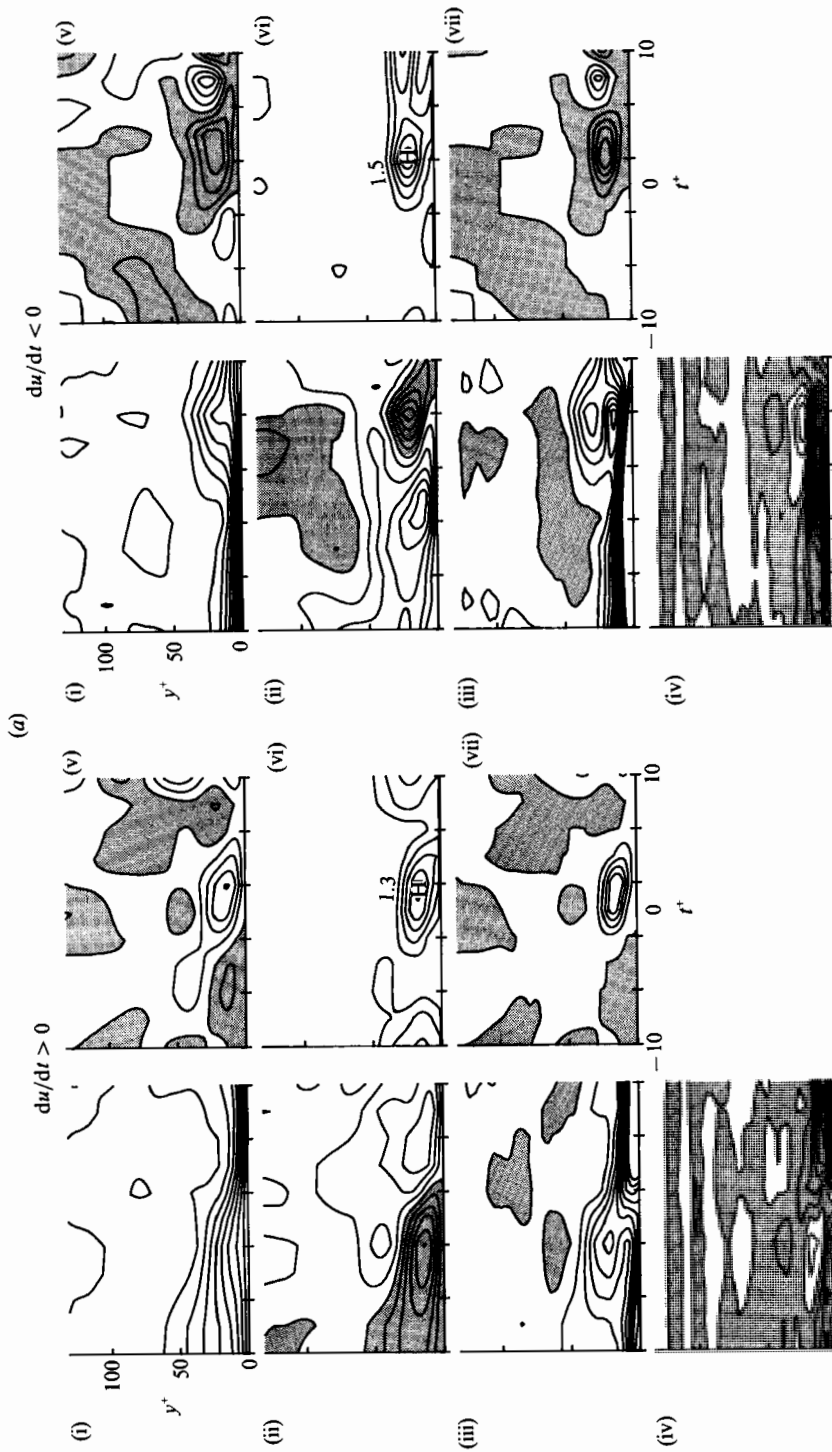
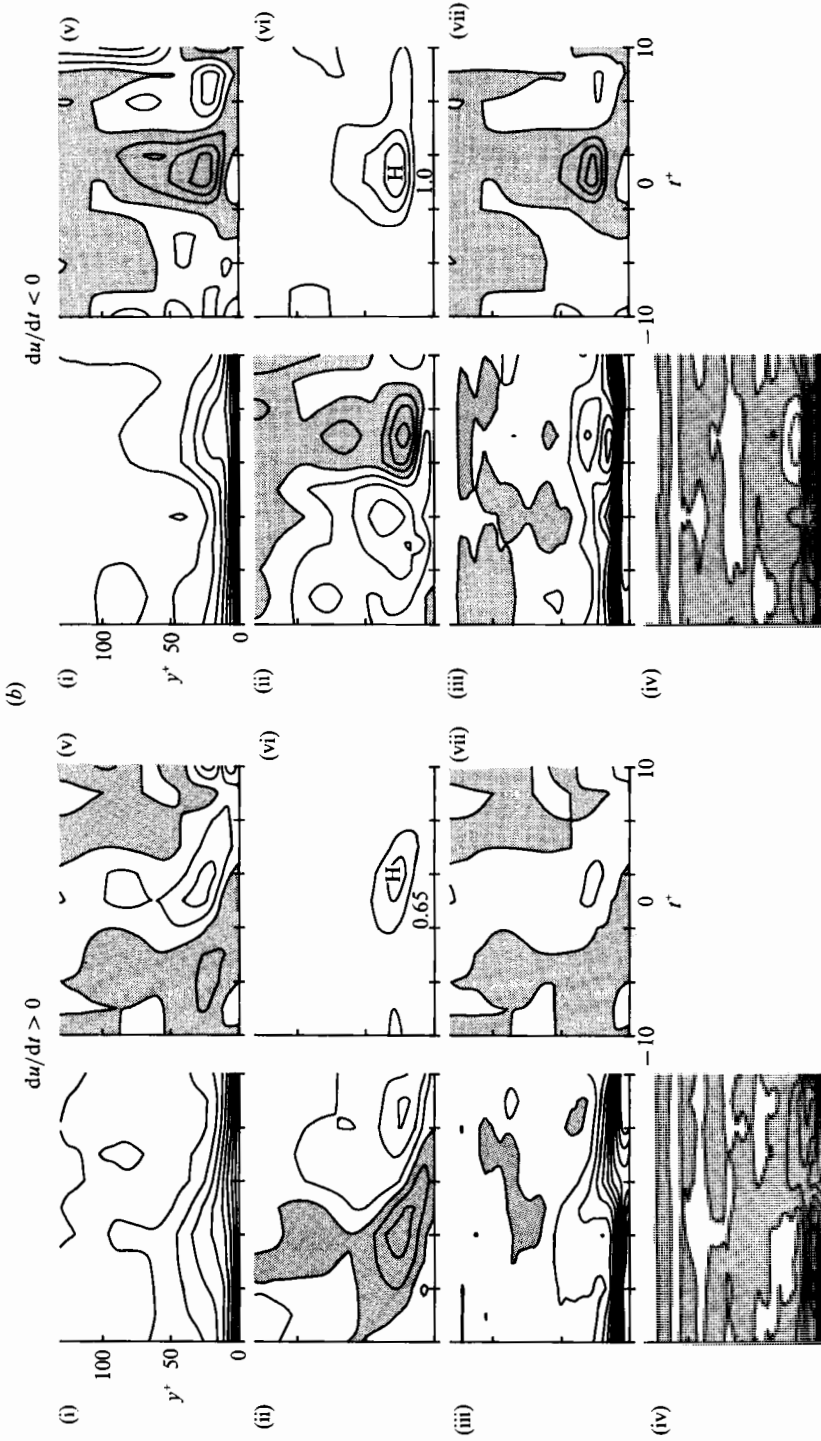


FIGURE 9(a). For caption see page 321.



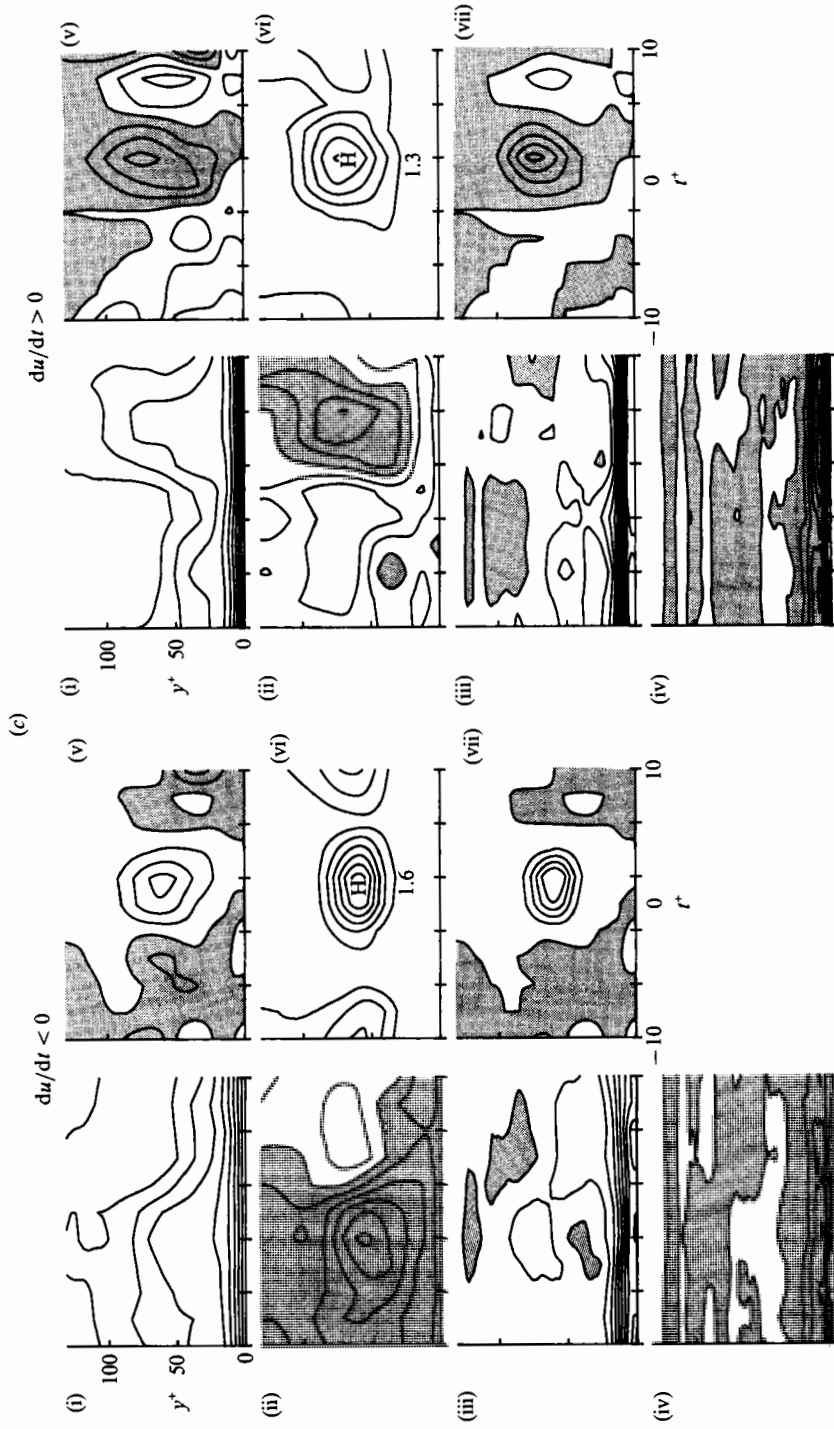


FIGURE 9. Conditional ensemble-averaged isocontours of velocity and velocity-derived properties. $k = 1$ at specified detection point. (i) u , (ii) u' , (iii) du/dy , (iv) d^2u/dy^2 , (v) du/dt , (vi) $VITA \times du/dt$, (vii) $VITA$, (viii) $VITA \times du/dt$. (a) $y^+ = 15$, (b) $y^+ = 30$, (c) $y^+ = 65$. Contour intervals as in figure 7.

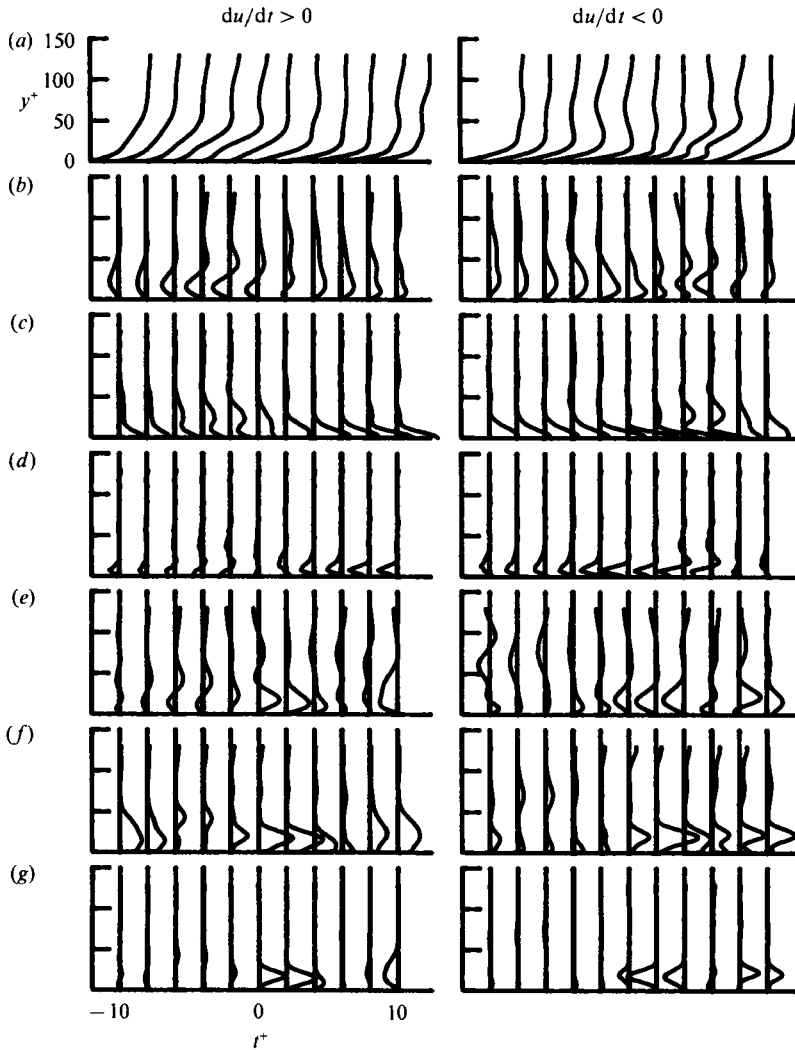


FIGURE 10. Conditional ensemble-averaged profiles of velocity and velocity-derived properties. $k = 1$ at $y^+ = 15$ (corresponds to figure 9a). (a) u , (b) u' , (c) du/dy , (d) du^2/dy^2 , (e) du/dt , (f) VITA, (g) $VITA \times du/dt$. Profile intervals as figure 6.

is a characteristic pattern for all the accelerated detections shown in figure 9. The patterns for the decelerated VITA detections are not nearly as systematic (partly owing to the low number of identified events in the sample); however, similar types of u' and $\partial u/\partial y$ patterns are present, although reversed in sign.

Note that several examples of the VITA-detected events used to compile the conditional ensemble averages of figure 9 are shown in figures 12–16. Examples of accelerated, decelerated, and multiple-ejection burst-type behaviour are shown, allowing comparison of velocity-derived property contours with the original visual sequence. These figures are discussed in detail in §5.3.

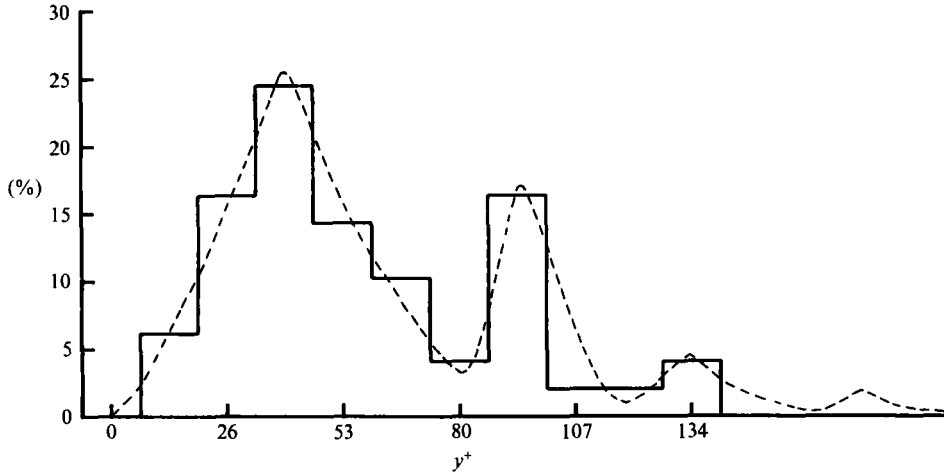


FIGURE 11. Probability distribution of burst-type events using regional peaks of VITA ≥ 1 .

5.2. Bursting times

Of recent concern and controversy has been the determination of average bursting times (i.e. the average time between detected burst-type events). The present data were evaluated for temporal bursting behaviour to examine their consistency with previous probe results.

A 'point' detection criterion employing the VITA parameter was used to establish 'averaged' bursting periods based on the threshold criteria of $k = 1$ and $\partial u/\partial t > 0$. Using this approach, the averaged bursting period for locations $y^+ = 15, 30, 65$ and 100 were established as $T^+ = 258, 272, 337,$ and 408 respectively. Note that the bursting period for the lower two locations is $T^+ \approx 260$, which is close to the bursting frequency $f^+ \approx 0.0035$ ($T^+ = 285$) suggested from the probe-rake results of Blackwelder & Haritonidis (1983). Furthermore, if threshold criteria of $k = 0.4$ and $\partial u/\partial t > 0$ are applied, similar to an approach employed by Luchik & Tiederman (1987), the averaging bursting time at detection points $y^+ = 15$ and 30 in the present data set decreases to $T^+ \approx 80$, which is comparable to $T^+ \approx 90$ suggested by Luchik & Tiederman.

Figure 11 was constructed from the VITA contour data to examine the distribution of the most active flow events with distance from the surface. This figure shows the distribution of the centres of closed VITA contours where VITA > 1 . The apparent trend is for the number of events to increase up to $y^+ \approx 30$ to 40 , and then decrease with further departure from the surface (note that the reason for the secondary peak at $y^+ \approx 95$ is unclear, but may be a sample-size effect). This variation of detected events with normal distance is somewhat similar to the bursting results obtained by Johansson & Alfredsson (1982) using single-probe detection (their detector probe was located progressively farther from the surface) where they also note a similar peak in the number of detected events around $y^+ \approx 30$ to 40 .

The probability distribution shown in figure 11 is also consistent with the concept of a turbulent boundary layer consisting of a hierarchy of hairpin vortex events as suggested by Perry & Chong (1982); they suggest a model where the occurrence of hairpins decreases and the scale increases with distance from the wall, which is similar to the behaviour of figure 11 for $y^+ \geq 30$. The suggested distribution is also supported by the results of a pattern-matching procedure for identifying hairpin

vortex patterns in turbulent boundary layers by Lu & Smith (1988) and Smith & Lu (1989). Lu and Smith indicate that detected hairpin-type patterns increase in scale and decrease in probability with distance from the wall. Note that if a bursting time is approximated based on the cumulative VITA events between $y^+ \approx 12$ and 39 in figure 11, which also satisfy $\partial u/\partial t > 0$, the averaged bursting time for this region is $T^+ \approx 88$, which is essentially the same as the $T^+ \approx 90$ bursting time suggested previously by Luchik & Tiederman (1987). Note that this type of regionalized evaluation is similar to the visual detection of bursts employed originally by both Kline *et al.* (1967) (who also suggested an average burst time comparable to $T^+ \approx 90$), and by Luchik & Tiederman (1987) employing a cross-comparison of dye ejections with probe detection techniques.

Clearly, the development of conditional space-time ensemble averages during VITA-detected burst-type behaviour provides a more detailed picture of the turbulence-generating patterns than similar analyses of pointwise probe measurements (even for the other detection techniques of uv , quadrant 2, and u -level). Considering the variety of detection techniques and criteria which have been employed for burst detection, it can be understood why significant discrepancies in determining bursting periods exist. The processes which occur in a turbulent boundary-layer flow display significant spatial-temporal scales which pointwise detections cannot properly establish; even the use of a rake of probes has spatial limitations.

Examination of individual cases for VITA-detected events suggests that the general behaviour of velocity and velocity-derived properties for these individual cases is similar to the results of the ensemble averages shown in the previous section, except for local variations in scales and amplitudes from case to case. The following section presents several typical examples of these space-time burst-type events, and illustrates how these spatial-temporal patterns may be categorized in terms of the respective isocontour and visualization patterns.

5.3. *Burst-type events: categorization*

As demonstrated in the previous sections, the present data set is quantitatively consistent with previous results for a typical turbulent boundary layer. Using the VITA detection procedure, these data have been used to illustrate the spatial-temporal ensemble behaviour of velocity properties in proximity to local probe-type event detections. However, as was suggested above, and pointed out in the original visual work on bursting by Kline *et al.* (1967), the detailed probe detection work of Tiederman (1989), and the numerical simulation work of Kim *et al.* (1987), bursting is regionalized behaviour which lends itself rather poorly to pointwise detection. Since the present data provide temporal velocity profile information in conjunction with simultaneous visualization data, an examination was done which suggested generalization of several types of burst-type events based on repetitive VITA contour patterns, the local acceleration/deceleration conditions, and the scales of the flow structure. To identify the type of 'burst' or event detected, the convolution of $VITA \times \partial u/\partial t$ is employed to indicate the occurrence of either an accelerated event ($VITA \times \partial u/\partial t > 0$) or a decelerated event ($VITA \times \partial u/\partial t < 0$). Individual sequences selected to illustrate specific types of VITA-detected behaviour appear in figures 12–17.

As shown in the ensemble averages of figures 8 and 9, a VITA-detected burst-type is characterized by either a slow deceleration followed by a sharp acceleration (accelerated event), or a slow acceleration followed by a sharp deceleration

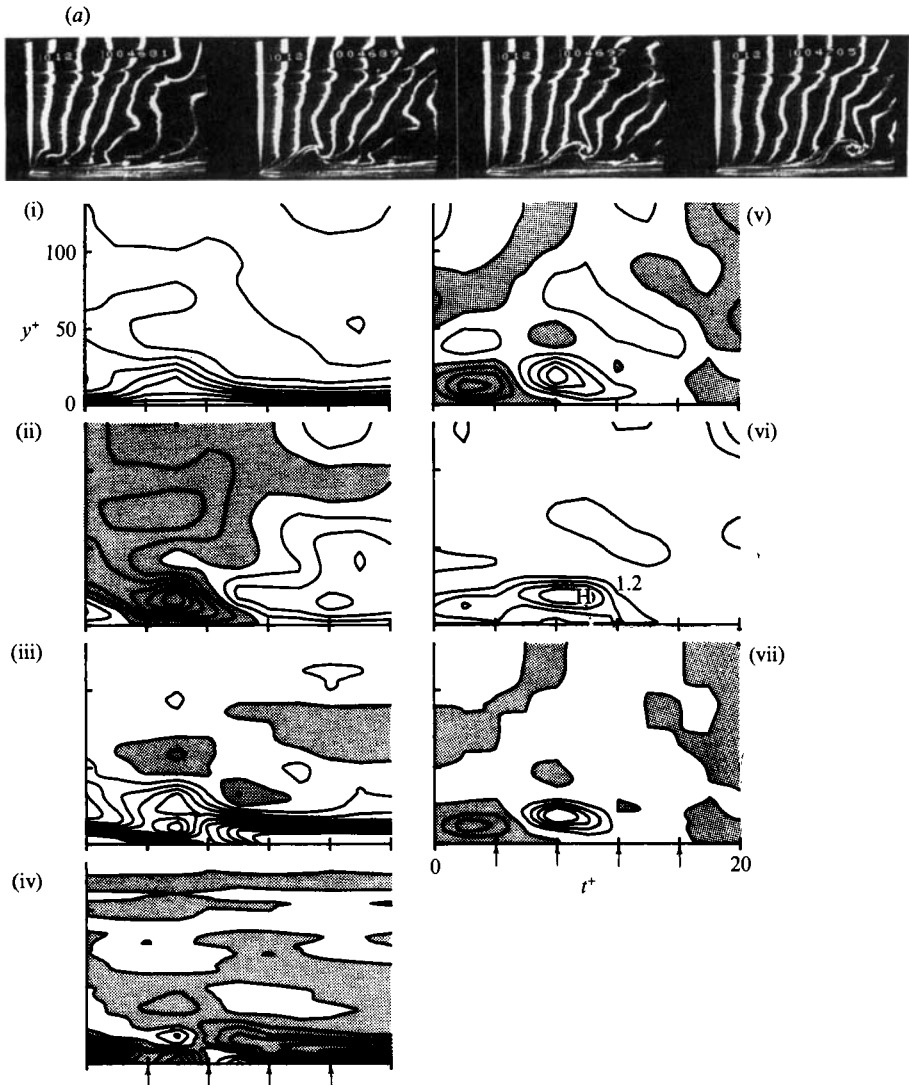


FIGURE 12(a). For caption see page 327.

(decelerated event). The former accelerated event ($\partial u/\partial t > 0$) is the one most commonly accepted as a true burst-type event, characterized as an ejection of low-momentum fluid from the surface, followed by a rapid acceleration or 'sweep' of high-momentum fluid. The latter decelerated event ($\partial u/\partial t < 0$) seems to reverse the sweep-ejection process, which is a bit perplexing since this does not fit the conventional bursting scenario. In most studies, these decelerated events are discounted when attempting to establish 'bursting' times, retaining only the accelerated events. However, in the present characterization, we have examined and characterized all events which demonstrate significant spatial-temporal activity as determined by a preselected $VITA > 1$ threshold. Note that the selection of $VITA > 1$ is arbitrary, but assures that the events selected are significant ones within the flow. Clearly, a lower threshold would modify the total number of events 'detected',

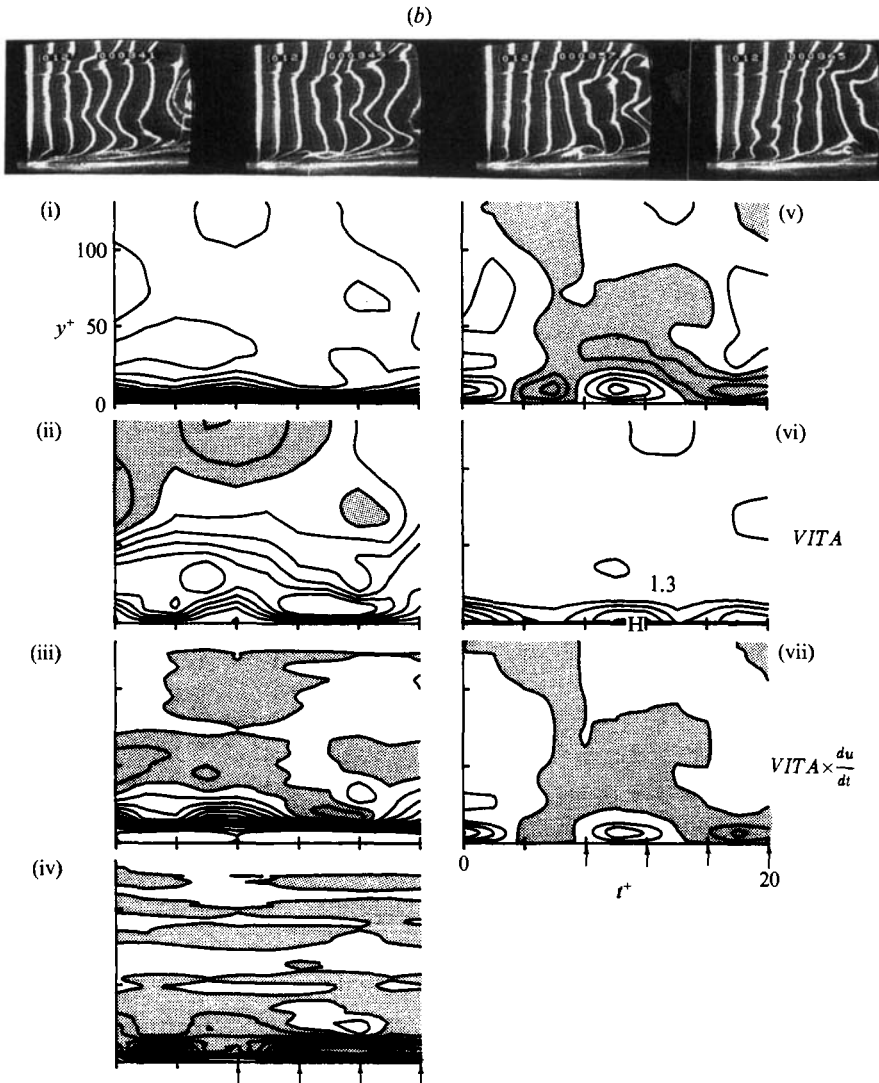


FIGURE 12(b). For caption see facing page.

but an examination of the data set indicates that such events are essentially similar in character and distribution to the events characterized below.

The types of events are broadly categorized as single detection, sequential detection, and parallel detection events, based on whether events occur in isolation or in close proximity to other events. Each category may be broken down further as representative of accelerated or decelerated events, or a combination. Even within each subcategory, significant variances in position, size, and intensity of events occur, as will be illustrated for several cases.

5.3.1. A Single VITA events

These are VITA-detected events characterized by a single set of closed VITA contours.

(i) *Accelerated event* Figure 12(a)–(c) is selected to illustrate burst-type events

(c)

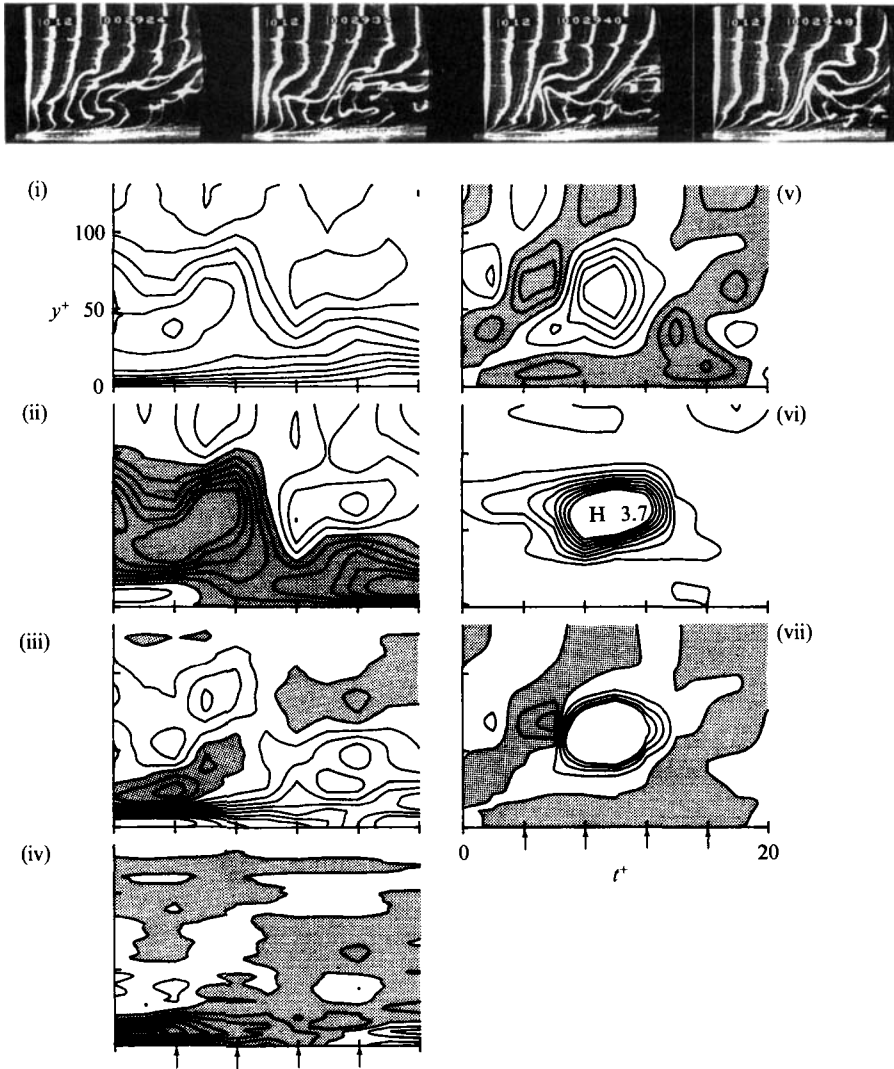


FIGURE 12. $VITA \geq 1$. (a) Single accelerated event, centred at $t^* = 1978$ in data sequence. (b) Smaller-scale, accelerated event, centred at $t^* = 54$ in data sequence. (c) Single accelerated event, centred at $t^* = 1100$ in data sequence. (i) u , (ii) u' , (iii) du/dy , (iv) d^2u/dy^2 , (v) du/dt , (vi) $VITA$, (vii) $VITA \times du/dt$. Contour intervals as in figure 7. The arrows below the isocontour plots in this and subsequent figures correspond to the temporal location of the respective picture in the accompanying visualization sequence.

which are similar to those detected by probe measurements and theoretical simulations (see Blackwelder & Kaplan 1976; Johansson & Alfredsson 1982; and Kim 1983). This accelerated-VITA detection is similar to the ejection/sweep-type motions described in previous studies. Note that all of these events are characterized by a single, closed VITA contour, with the maximum value occurring at the 'H' labelled in the contour (the value of H is listed near it). Three different sequences are shown which are relatively characteristic of this most common burst-type detection (approximately 40% of all characterized events in the data sequence). The first two sequences (figures 12a and 12b) illustrate typical near-wall detections, with the

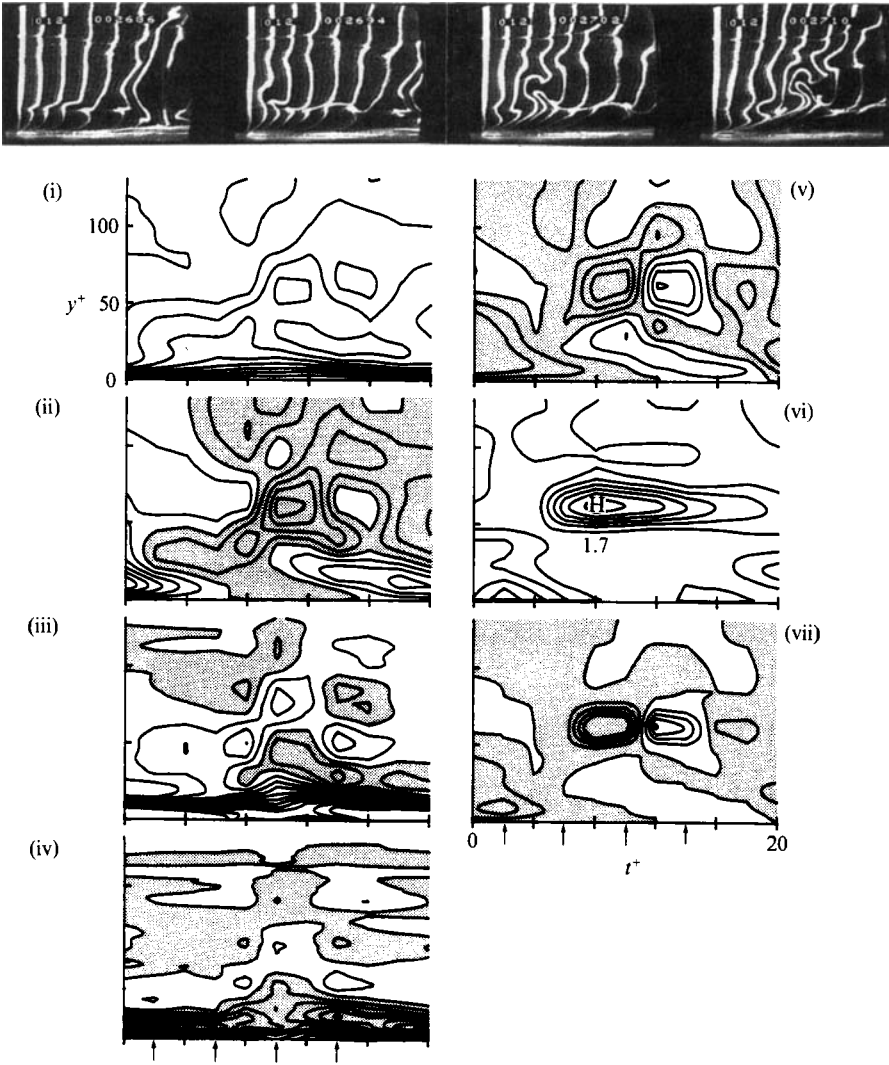


FIGURE 13. Single decelerated/accelerated event, $VITA \geq 1$. Centred at $t^+ = 978$ in data sequence. (i) u , (ii) u' , (iii) du/dy , (iv) d^2u/dy^2 , (v) du/dt , (vi) $VITA$, (vii) $VITA \times du/dt$. Contour intervals as in figure 7.

maximum located at $y^+ \leq 20$, and are most likely characteristic of most probe-detected events at the typical sampling location of $y^+ = 15$. Note that near the surface in figure 12(a), a bubble-line pattern develops which is characteristic of the transverse head of a hairpin vortex (Smith & Lu 1989). A similar pattern, only much less pronounced, can also be seen in figure 12(b). Figure 12(c) illustrates both the magnitude and extent of larger detected events farther removed from the surface, revealing a very large structure of significant activity and extent centred at approximately $y^+ = 60$ from the surface. Note that the visualization again displays a bubble-line pattern characteristic of a transverse vortex. Although clearly a dominant disturbance, it is apparent from the $VITA$ contour in figure 12(b) that such a structure would not be detected by a conventionally located probe. In general, such large *detected* events ($VITA > 1$) were less common than events occurring nearer the surface, as shown in figure 11.

(ii) *Decelerated events* Figure 13 illustrates a detected event consisting of a strongly decelerated velocity front, followed immediately by a somewhat comparable acceleration, resulting in a single event consisting of a combination of a sharp deceleration followed by a sharp acceleration, as shown in the $VITA \times \partial u / \partial t$ contours. Because the VITA is strongest during the deceleration stage, this is characterized as a decelerated event. Other similar events were observed for which the deceleration exceeded the acceleration phase, but this general type of event constituted only about 15% of all characterized events. The rationale for this type of event is illustrated to some degree in the visualization accompanying this figure. Note that the bubble-line pattern suggests a very significant retardation of the fluid near the surface, followed by what again appears to be the development of a transverse vortex pattern and a subsequent acceleration of the flow. In many respects the visualization pattern is not dissimilar to those shown in figures 12(a) and 12(c), but exhibits variations in the magnitude of the particular acceleration and deceleration phases, which results in a recategorization of this pattern as a deceleration-dominant pattern. For whatever reason, these types of detections suggest that a sudden, rapid deceleration of the local wall fluid exceeds the subsequent recovery and reacceleration of the flow. In general, the flow patterns for this type of event do not appear markedly dissimilar from the accelerated type of events (if one accounts for scale), suggesting that detected accelerated and decelerated events may be the product of similar processes which are not appropriately discriminated by weighting detected VITA events according to the local sign of $\partial u / \partial t$.

5.3.2. Sequential dual VITA events

These are dual events characterized by a pair of closed VITA contours which are temporally close ($\Delta t^+ < 15$) and aligned at essentially the same distance from the surface, suggesting one combined or two separate, but associated, sequential events of similar scale. One reason for the appearance of the dual VITA contours could be that the averaging time interval employed for calculation of the VITA parameter is less than the timescale of the total burst event. However, as shown in figure 14, a dual event sequence can be the result of an extended burst-type event characteristic of a multiple-ejection burst-type event as originally described by Bogard & Tiederman (1986) from probe studies and more recently observed by Robinson *et al.* (1989) in their detailed characterization of the numerical simulation data base of Spalart (1988). In the present study, it was observed that these type of sequenced events generally have a maximum centred at $y^+ > 20$, such that conventional probe measurements at $y^+ = 15$ might be less likely to detect them. In general, these sequenced events made up approximately 25% of all characterized events.

(i) *Aligned decelerated/accelerated events* Figures 14(a) and 14(b) illustrate a sequence consisting of combined dual VITA events, essentially similar in behaviour and visual appearance to the single VITA decelerated event shown in figure 13. The essential difference between these figures is that figures 14(a) and 14(b) have a longer interaction period than a single detection case. However, note that all three of these sequences characterize the complete burst cycle observed visually by Kline *et al.* (1967), Kim *et al.* (1971), and Offen & Kline (1974), comprised of a lift-up (deceleration) followed by an ejection/sweep motion (acceleration). This particular type of dual detection case is the result of a burst-type event, with both strong deceleration and acceleration phases which extend beyond the VITA averaging time employed. Thus both the initial deceleration and subsequent acceleration both

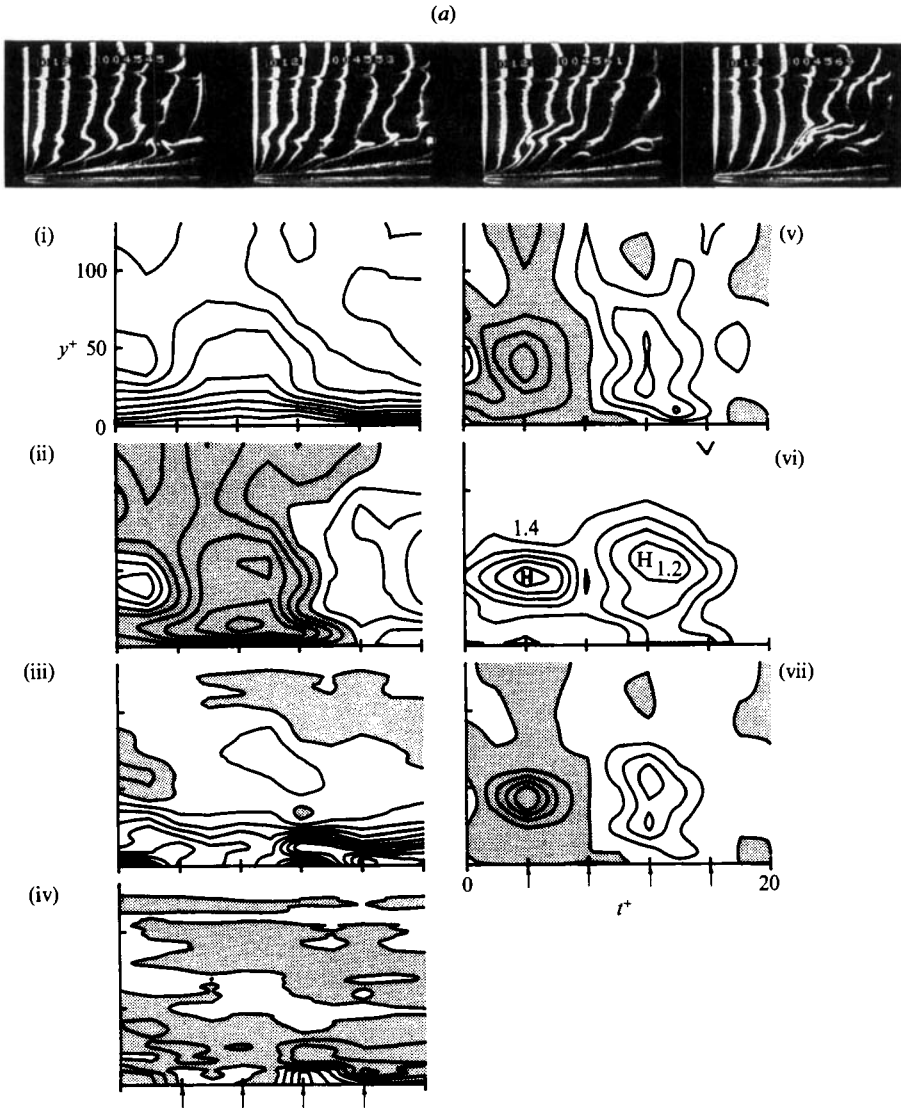


FIGURE 14(a). For caption see page 333.

appear as detected events. Note from the captions of figures 14(a) and 14(b) that these two sequences are separated in the total data sequence by only $\Delta t^+ = 28$, and are in essence part of a burst-type sequence consisting of several multiple ejections spanning a time of $\Delta t^+ \approx 50$.

(ii) *Aligned accelerated/decelerated events* Figure 14(c) shows two closely aligned VITA detections separated by $\Delta t^+ = 8$. The initial accelerated event reflects (see the first half of the visual sequence) an ejection/sweep-like motion, quite similar to figure 12(a), followed closely by a strong deceleration, corresponding to the second VITA event (quite similar to figure 13; compare fourth picture in 14(c) to first picture in 13), which is indicative of a lift-up of low-speed fluid. Note that in this dual detection sequence the accelerated phase precedes the deceleration phase, in opposition to conventionally expected behaviour. This is because the detected events are again a part of a multiple-ejection sequence. The detection of the initial accelerated event is

(b)

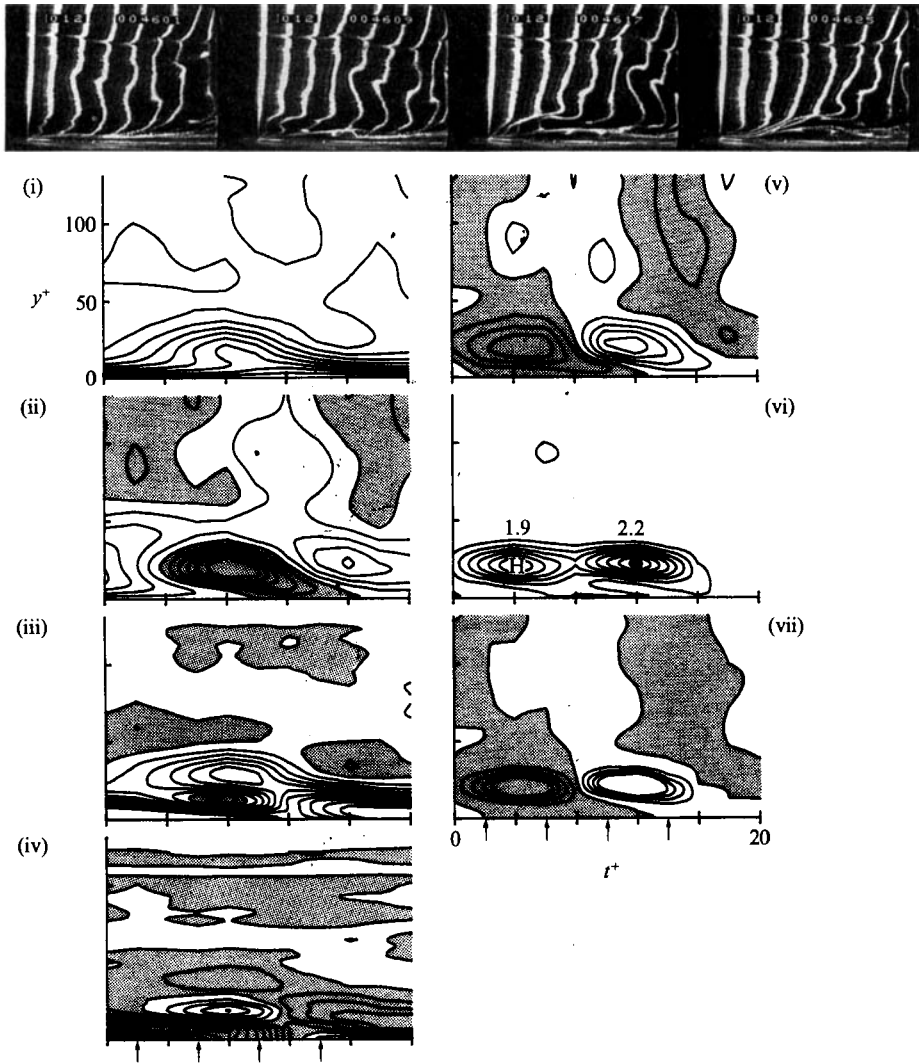


FIGURE 14(b). For caption see page 333.

conventional, with the preceding deceleration being sufficiently weak not to trigger the threshold detection; however, a strong deceleration follows immediately on the heels of the accelerated event, which is also detected as a $VITA > 1$ event.

(iii) *Aligned accelerated/accelerated events* Figure 14(d) illustrates a dual-event sequence which again reflects a multiple-ejection burst-type sequence. This sequence consists of two detected accelerated events occurring in close proximity within a multiple-ejection process. Note that the $\partial u/\partial t$ contours indicate that the flow undergoes an alternating deceleration/acceleration/deceleration/acceleration etc. process, with the accelerated phases markedly stronger than the decelerated phases. This type of generic behaviour in a burst-type process was illustrated originally in a study of single-probe burst detection by Wallace, Brodkey & Eckelmann (1977), wherein they showed that a decelerated region always separates each accelerated event in a burst-type sequence. Again, this burst-type event subcategory reflects the

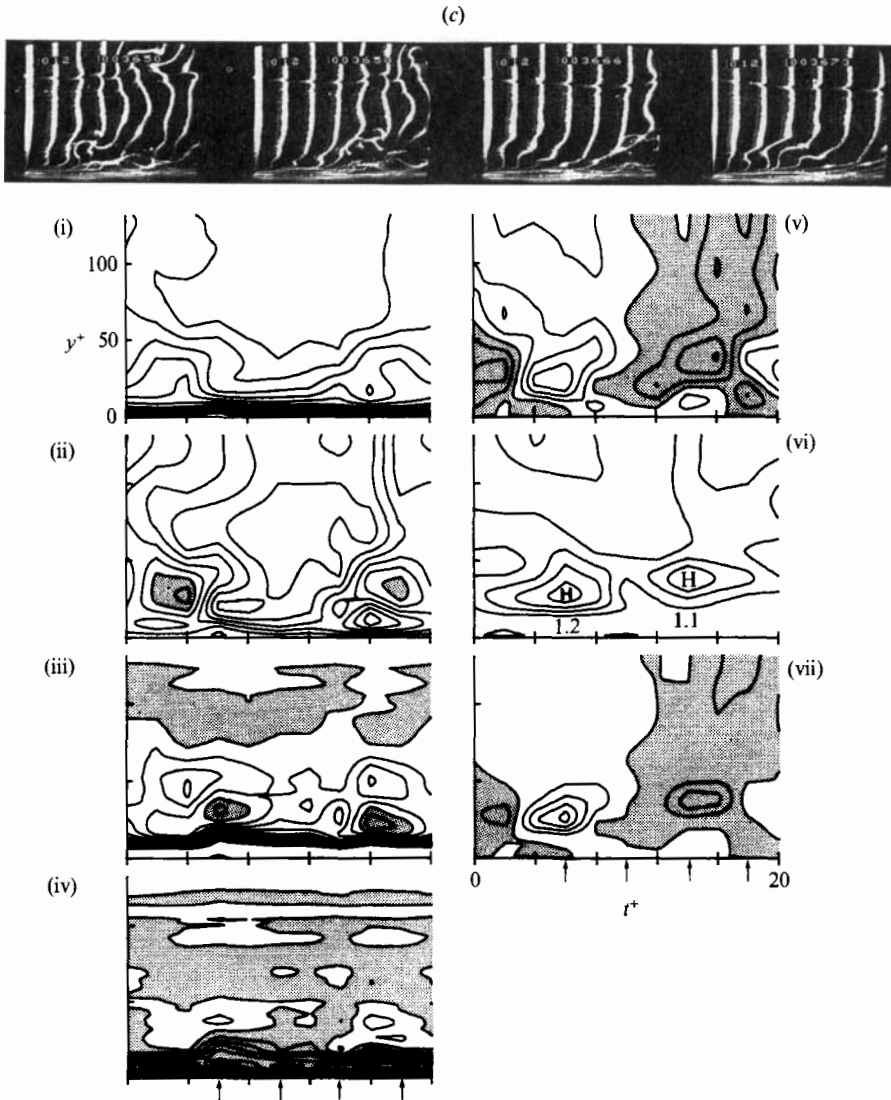


FIGURE 14(c). For caption see facing page.

way in which similar visual behaviour (note the similarity of the last visualization pictures in figures 14*a*, 14*d*, and 12*c*), can yield markedly different quantitative characteristics.

For the entire data set, various combinations of sequenced events could be detected. Clearly, the type of sequence detected will depend strongly upon the intercomplexities of the multiple ejections within a burst-type event, the averaging time, and the level of threshold detection. This second category of burst-type behaviour is a general reflection of the multiple-ejection burst-type events identified originally by Bogard & Tiederman (1986), and extended by Luchik & Tiederman (1987).

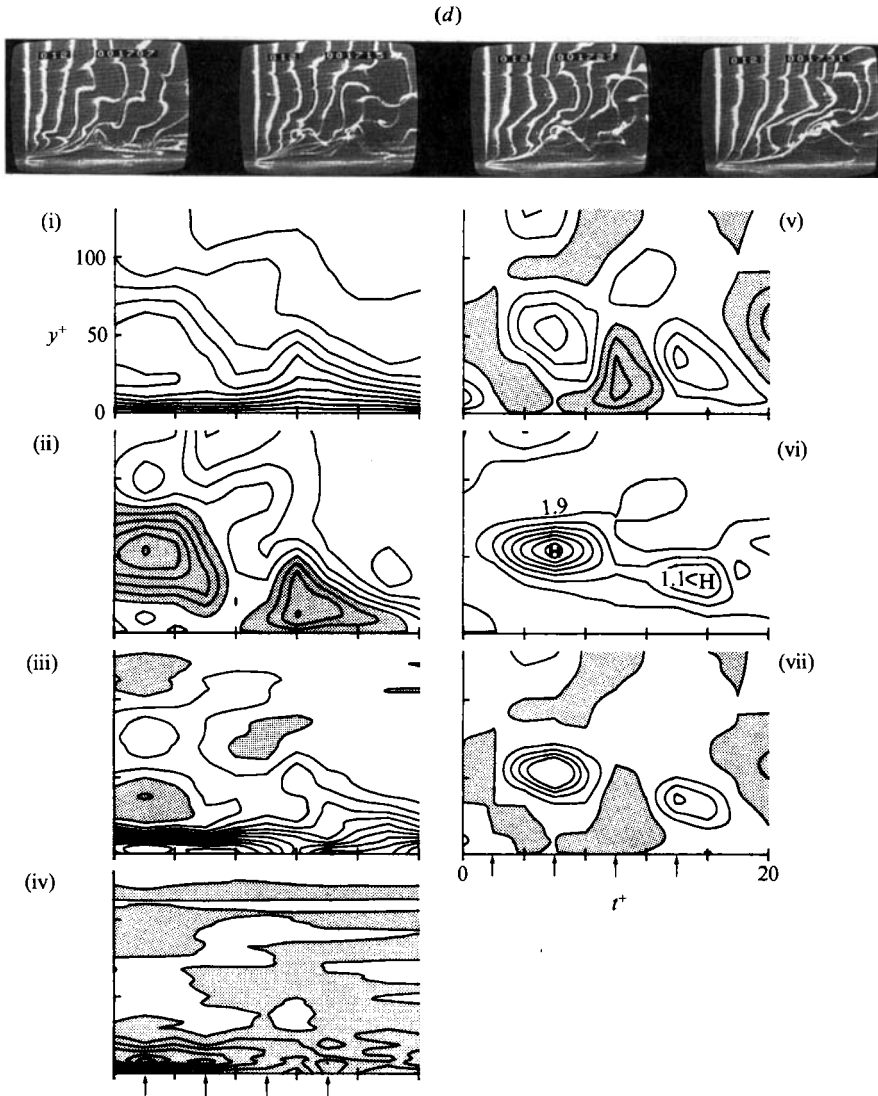


FIGURE 14. Double $VITA \geq 1$. (a) aligned decelerated/accelerated events, centred at $t^* = 1910$ in data sequence; (b) aligned decelerated/accelerated events, centred at $t^* = 1938$ in data sequence; (c) aligned accelerated/decelerated events, centred at $t^* = 1460$ in data sequence; (d) aligned accelerated events, centred at $t^* = 498$ in data sequence. (i) u , (ii) u' , (iii) du/dy , (iv) d^2u/dy^2 , (v) du/dt , (vi) $VITA$, (vii) $VITA \times du/dt$. Contour intervals as in figure 7.

5.3.3. Parallel double $VITA$ events

These are two detected events characterized by a pair of separate, closed $VITA$ contours which essentially parallel each other at different heights above the surface, as shown in figure 15. These detected events suggest two associated events of differing scales, or one larger event with two defined regions of activity. Although segregation of these types of events from the other categories was somewhat subjective, they appeared to comprise approximately 20% of all characterized events.

(i) *Parallel accelerated/accelerated events* Two parallel accelerated events asso-

(a)

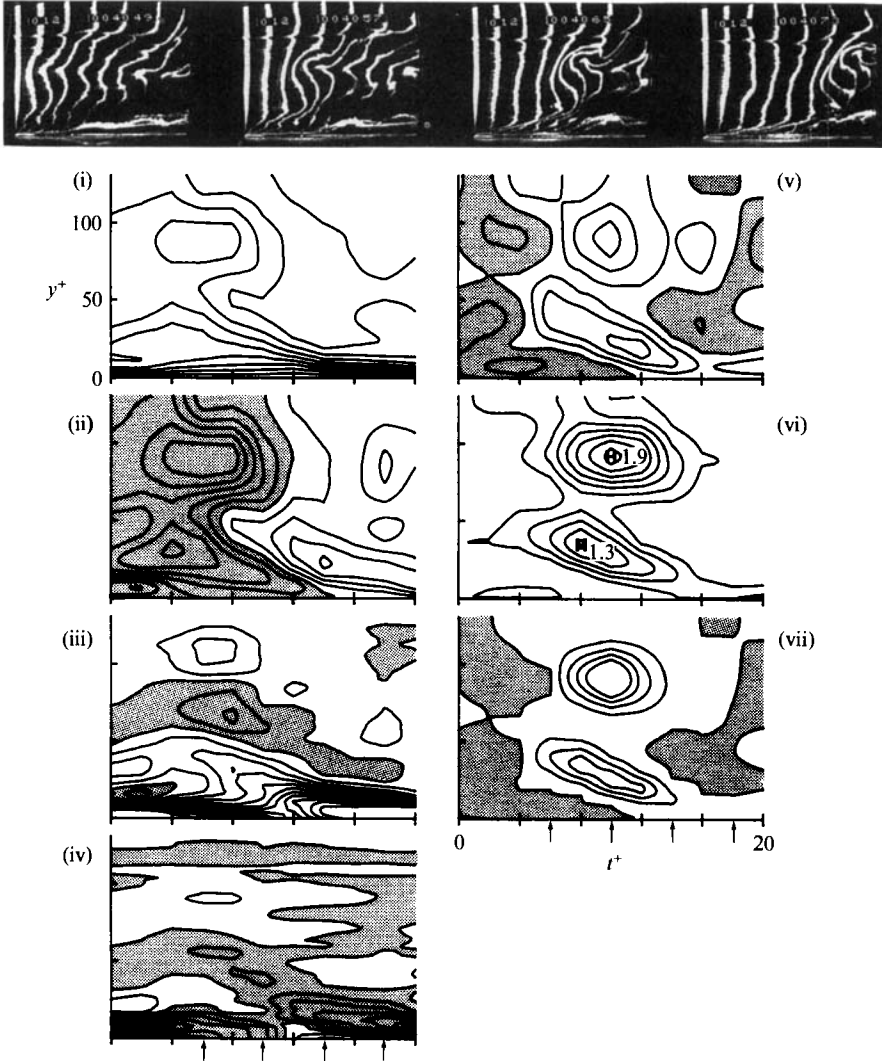


FIGURE 15(a). For caption see facing page.

ciated with the passage of an apparent large-scale structure are shown in figure 15(a). Note that both the visualization pictures and the quantitative contours suggest that this is essentially the classic probe-detected burst-type behaviour of a slow deceleration/strong acceleration on a very large scale (extending outward beyond $y^+ = 100$). Note that in the case shown, the outer detection is markedly stronger than the inner detection, which is generally the case. The rationale for the two separate, but associated, regions may be the stimulation of the inner event by the outer event. The outer bubble pattern does display the characteristics of a large transverse vortex (possibly a hairpin head), which has been suggested by Smith *et al.* (1990), Walker (1990), and Robinson *et al.* (1989), among others as the stimulus for turbulence-generating surface eruptions.

(ii) *Parallel decelerated/accelerated events* Figure 15(b) illustrates another form of parallel events with the outer event reflecting a strong decelerated event in close

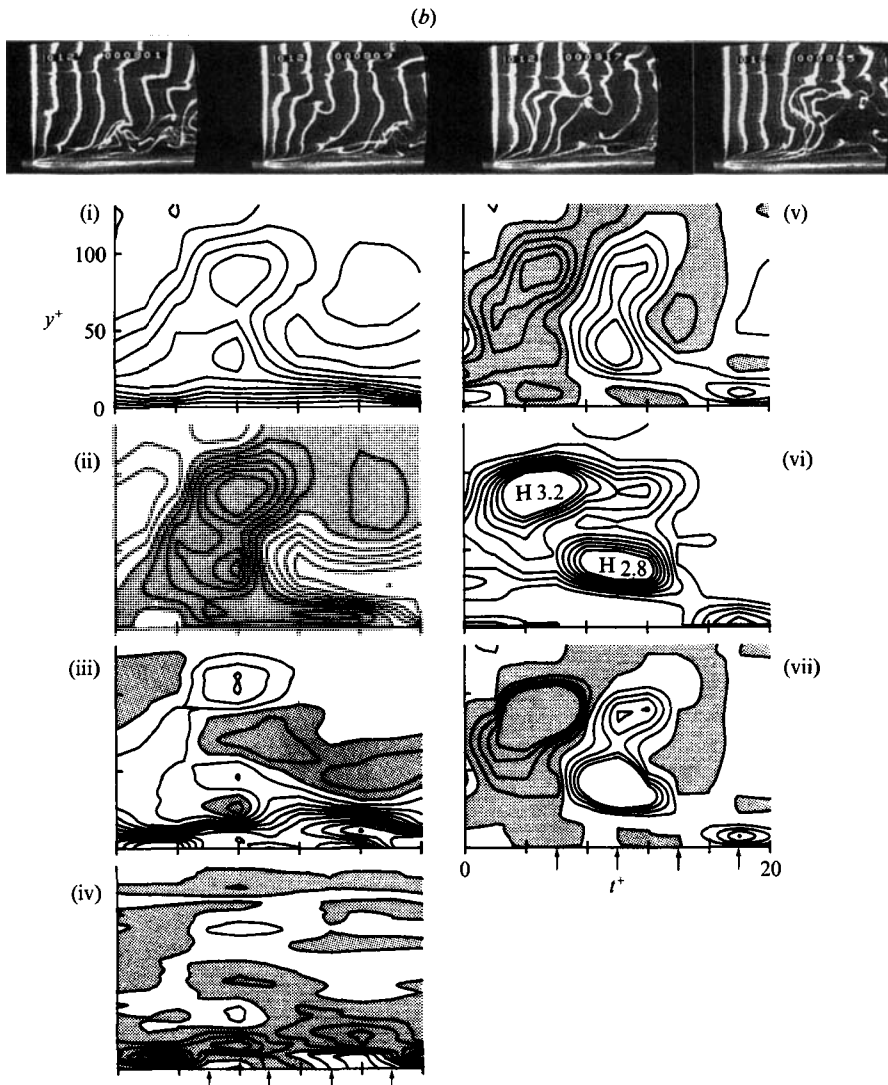


FIGURE 15. Double $VITA \geq 1$: parallel accelerated/accelerated events, centred at $t^+ = 1660$ in data sequence; (b) parallel accelerated/decelerated events, centred at $t^+ = 36$ in data sequence. (i) u , (ii) u' , (iii) du/dy , (iv) d^2u/dy^2 , (v) du/dt , (vi) $VITA$, (vii) $VITA \times du/dt$. Contour intervals as in figure 7.

proximity to an inner accelerated event. The bubble-line patterns again crudely suggest a large transverse vortical structure, which could be associated with the strong deceleration in the outer region, with the subsequent acceleration reflecting a sweep motion following in the wake of the transverse vortex and impinging toward the surface to yield the accelerated detection.

Clearly, these parallel events seem to be interconnected in some form of complicated, large-scale structure extending to $y^+ \approx 100$ or more. These events are of significantly broader expanse, and yield higher $VITA$ maxima than the more compact single-event detections. It is worthwhile to note that these types of parallel events bear some similarity to the hairpin hierarchy model suggested by Perry &

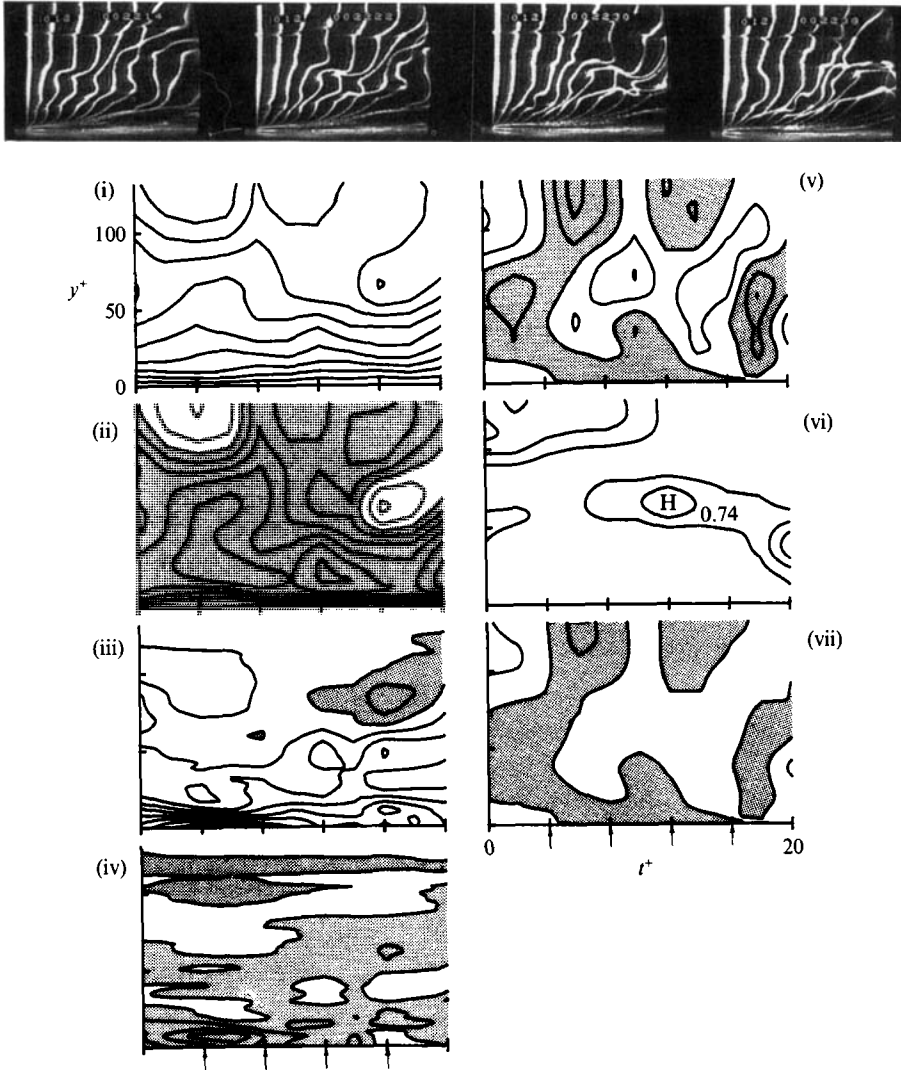


FIGURE 16. Burst-type event established by visualization; $VITA < 1$, centred at $t^+ = 742$ in data sequence. (i) u , (ii) u' , (iii) du/dy , (iv) d^2u/dy^2 , (v) du/dt , (vi) $VITA$, (vii) $VITA \times du/dt$. Contour intervals as in figure 7.

Chong (1982), wherein they assume a growth of scales through the continued, systematic evolution of smaller hairpins into larger hairpin structures.

5.3.4. Visual detection with $VITA < 1$

As was pointed out above, the use of an arbitrary threshold as a detector biases the types of events detected; in some cases, what appear to be rather obvious visual burst-type events may miss detection. This is illustrated by the visualization sequence in figure 16, which suggests the presence of a burst-like event similar to those in figure 15, but which the $VITA$ contours indicate as an accelerated event of $VITA < 1$. As shown previously by Luchik & Tiederman (1987), and as illustrated by the 'apparent' visually detected burst-type event shown in figure 16, the detection of 'bursting' events is strongly affected by the selection of the detection parameters,

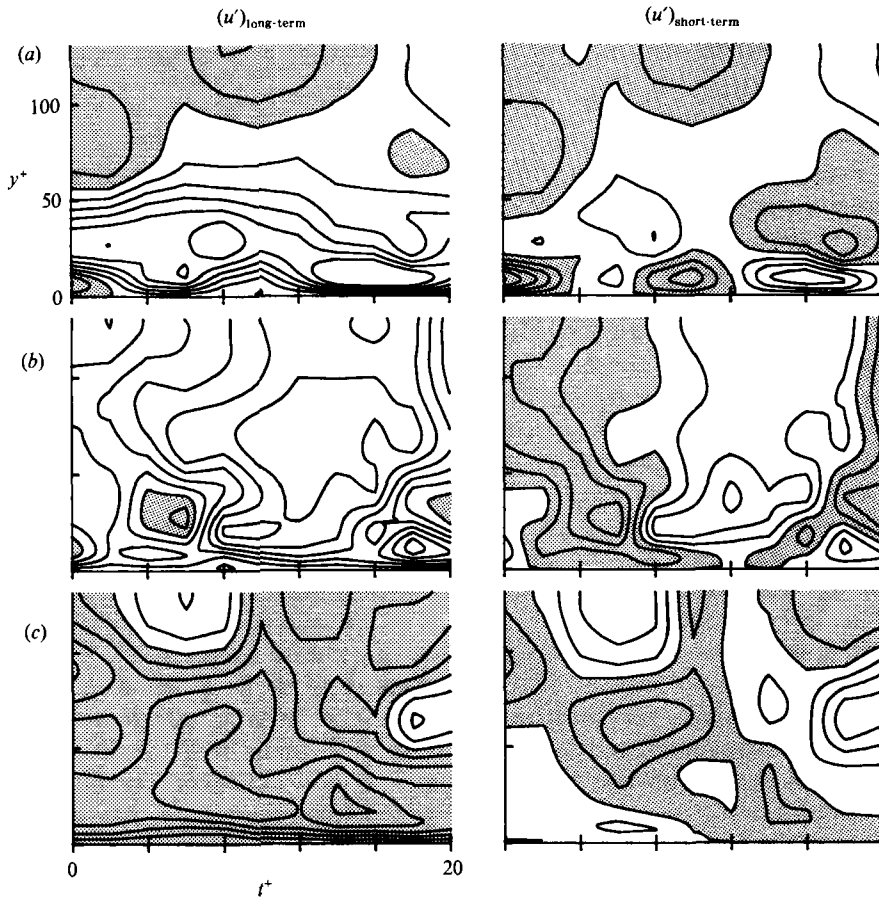


FIGURE 17. Comparison of velocity variations relative to both the long-term (conventional) and short-term (over $\Delta T^+ = 22$) mean velocity. Selected sequences from turbulent-boundary-layer data set. (a) $t^+ = 54$, corresponding to figure 12 (b). (b) $t^+ = 1460$, corresponding to figure 14 (c). (c) $t^+ = 742$, corresponding to figure 16. Contour intervals as in figure 7.

such that the detection of an event depends significantly on the choice of both the averaging-time interval (T^+) and the VITA threshold considered as indicative of a burst-type event.

5.4. Short-time variations

Integral to the VITA detection approach is the examination of the local short-time behaviour of the turbulent boundary layer in order to determine 'local' events or activity. Note that this approach examines the fluctuations about a local short-time mean; an approach shown to be of particular utility by Wallace *et al.* (1977) in enhancing the use of quadrant splitting for the detection of burst-type events using single probe measurements. This concept of examining and establishing velocity excursions from *local* mean behaviour appears particularly important in establishing regional variations in flow behaviour. Figure 17 is shown to illustrate the difference between fluctuations about long-term and short-term averages. This figure shows three selected sequences from the turbulent-boundary-layer data set; from the comparison of short-term and long-term variations, it is clear how the use of short-term variations better reveals local, active events. (This concept of local fluctuation behaviour is also key to the proper employment of regional matching and correlation

schemes for 'finding' hairpin vortices in turbulent boundary layers (Lu & Smith 1988; Smith & Lu 1989).

6. Concluding remarks

As has been shown in the present study, the use of the VITA technique with its local averaging and threshold detection constraints can properly detect some of the burst-type events. However, because it is a pointwise detection procedure, the conventional VITA detection procedure cannot effectively detect 'distributed' burst-type events occurring over space.

From the present work it appears that the deceleration/acceleration type of event which has been previously characterized as typical 'burst' behaviour (Blackwelder & Kaplan 1976), is more accurately characterized in two dimensions by ascending/descending 'hump-shaped' velocity contours, indicative of expanded decelerating/accelerating velocity fronts (similar to the 'lift-up/ejection/sweep' process suggested by previous visual studies). However, the present study also suggests that burst-type events or regions of local activity may take on a number of different characteristic patterns in two dimensions, although it is unclear whether all such patterns can be accurately termed turbulence-producing bursts. Note that if it is assumed that each closed $VITA \geq 1$ contour over the range $0 < y^+ \leq 135$ and $0 < t^+ < 2024$ represented a burst detection, the resulting 'averaged' bursting period would be $T^+ \approx 36$, much lower than the results quoted for VITA detections at pointwise locations. If we make adjustments to account for multiple ejection-type events, which cause over-counting, the resulting averaged burst period would increase to $T^+ \approx 55$, still much lower than most conventionally discussed burst periods. However, one must realize that the use of a detection criterion well-removed from the surface has an unclear meaning since the term burst has come to characterize a region of local activity associated with a turbulence-generating event, which must occur close to the surface. In addition, the results illustrated in §5.3.4 clearly illustrate that the detection or non-detection of events is strongly biased by the selection of the averaging time window and the detection threshold, resulting in the under- and/or over-detection of burst-type events by the VITA technique.

Because of the three-dimensional complexity of scales that are associated with turbulent boundary layers, an appropriate burst detection approach must provide for variations in scales of both time and length. This point is also reinforced by the careful characterization of the numerically simulated boundary layer by Robinson *et al.* (1989). It would appear that the appropriate approach should utilize some form of 'regional' detection technique which is keyed on a particular quantitative pattern to be identified. Such an approach has been explored (Lu & Smith 1988; Smith & Lu 1989) using the spatial-temporal characteristics of hairpin vortices as a pattern indicative of turbulence-generation within a turbulent boundary layer. This method of pattern matching within spatial-temporal velocity fields is the topic of a more extensive paper to appear shortly.

The authors wish to thank Dr J. David A. Walker, Dr A. H. Haidari, and Mr E. V. Bacher for their advice and assistance. We also wish to thank the Air Force Office of Scientific Research for its support of this research. The continuing support of the AFOSR is gratefully acknowledged.

REFERENCES

- ABERNATHY, F. H., BERTSCHY, J. R. & CHIN, R. W. 1977 Turbulent spectra using laser-Doppler anemometry and selective seeding. In *Proc. 5th Symp. on Turbulence* (ed. G. K. Patterson and J. L. Zakin), p. 133. University of Missouri-Rolla.
- ALFREDSSON, P. H. & JOHANSSON, A. V. 1984 Time scales in turbulent channel flow. *Physics of Fluids*, **27**, 1974.
- BLACKWELDER, R. F. & HARITONIDIS, J. H. 1983 Scaling of the bursting frequency in turbulent boundary layers. *J. Fluid Mech.* **132**, 87.
- BLACKWELDER, R. F. & KAPLAN, R. E. 1976 On the wall structure of the turbulent boundary layer. *J. Fluid Mech.* **76**, 89.
- BOGARD, D. G. & TIEDERMAN, W. G. 1986 Burst detection with single-point velocity measurements. *J. Fluid Mech.* **162**, 389.
- CERRA, A. W. & SMITH, C. R. 1983 Experimental observation of vortex ring interaction with fluid adjacent to a surface. *Rep. FM-11*. Dept. of ME and Mech., Lehigh University.
- CLUTTER, D. W., SMITH, A. M. O. & BRAZIER, J. F. 1961 Techniques of flow visualization using water as the working medium. *Aerospace Engng* **20**, January.
- CORINO, E. R. & BRODKEY, R. S. 1969 A visual investigation of the wall region in turbulent flow. *J. Fluid Mech.* **37**, 1.
- CORNELIUS, K., TAKENCHI, K. & DEUTSCH, S. 1977 Turbulent flow visualization: a technique for extracting accurate quantitative information. *Proc. 5th Symp. on Turbulence* (ed. J. L. Zakin & G. K. Patterson), p. 287. Univ. Missouri-Rolla.
- DAVIS, W. & FOX, R. W. 1966 An evaluation of the hydrogen bubble technique for the quantitative determination of the fluid velocities within clear tubes. *ASME Paper 66-WA/E-21*.
- ECKELMANN, H., NYCHAS, S. G., BRODKEY, R. S. & WALLACE, J. M. 1977 Vorticity and turbulence production in pattern recognized turbulent flow structures. *Phys. Fluids* **20**, S225.
- GRASS, A. J. 1971 Structural features of turbulent flow over smooth and rough boundaries. *J. Fluid Mech.* **50**, 233.
- HOGENES, J. H. A. & HANRATTY, T. J. 1982 The use of multiple wall probes to identify coherent flow patterns in the viscous wall region. *J. Fluid Mech.* **124**, 363.
- JIMENEZ, J., MOIN P., MOSER, R. & KEEFE, L. 1988 Ejection mechanisms in the sublayer of a turbulent channel. *Phys. Fluids* **31**, 1311.
- JOHANSEN, J. B. & SMITH, C. R. 1983 The effects of cylindrical surface modifications on turbulent boundary layers. *Rep. FM-3*. Dept. of Mech. Engrg. and Mech., Lehigh University.
- JOHANSSON, A. V. & ALFREDSSON, P. H. 1982 On the structure of turbulent channel flow. *J. Fluid Mech.* **122**, 259.
- JOHANSSON, A. V., ALFREDSSON, P. H. & KIM, J. 1989 Velocity and pressure fields associated with near-wall turbulence structures. *Proc. Zaric Intl Seminar on Wall Turbulence* (ed. S. J. Kline) Hemisphere.
- JOHANSSON, A. V., HER, J. Y. & HARITONIDIS, J. H. 1987 On the generation of high-amplitude wall-pressure peaks in turbulent boundary layers and spots. *J. Fluid Mech.* **175**, 119.
- KASAGI, N., HIRATA, M. & NISHINO, K. 1986 Streamwise pseudo vortical structures and associated vorticity in the near-wall region of a wall-bounded turbulent shear flow. *Exps. Fluids* **4**, 309.
- KIM, H. T., KLINE, S. J. & REYNOLDS, W. S. 1971 The production of turbulence near a smooth wall in a turbulent boundary layer. *J. Fluid Mech.* **50**, 133.
- KIM, J. 1983 On the structure of wall-bounded turbulent flow. *Phys. Fluids* **26**, 2088.
- KIM, J., MOIN, P. & MOSER, R. 1987 Turbulence statistics in fully developed channel flow at low Reynolds number. *J. Fluid Mech.* **177**, 133.
- KLINE, S. J., REYNOLDS, W. C., SCHRAUB, F. A. & RUNSTADLER, P. W. 1967 The structure of turbulent boundary layers. *J. Fluid Mech.* **95**, 741.
- LU, L. J. 1985 Image processing of hydrogen bubble flow visualization for determination of turbulence statistics and bursting characteristics. M.S. thesis, Lehigh University.
- LU, L. J. & SMITH, C. R. 1985 Image processing of hydrogen bubble flow visualization for determination of turbulence statistics and bursting characteristics. *Exps. Fluids* **3**, 349.

- LU, L. J. & SMITH, C. R. 1988 Image processing of hydrogen bubble flow visualization for quantitative evaluation of hairpin-type vortices as a flow structure of turbulent boundary layers. *Rep. FM-14*. Dept. of Mech. Engrg and Mech., Lehigh University.
- LU, L. J. & SMITH, C. R. 1991 The application of orthogonal decomposition techniques as a smoothing filter for experimentally acquired temporal velocity profile data. *Exps. Fluids* (in press).
- LUCHIK, T. S. & TIEDERMAN, W. G. 1987 Timescale and structure of ejections and bursts in turbulent channel flow. *J. Fluid Mech.* **174**, 529.
- LUMLEY, J. L. 1967 The structure of inhomogeneous turbulent flows. In *Atmospheric Turbulence and Radio Wave Propagation* (ed. A. M. Yaglom & V. I. Tatarski), p. 166. Moscow: Nauka.
- METZLER, S. P. 1980 Processes in the wall region of a turbulent boundary layer. M.S. thesis, Dept. of Mech. Engrg and Mech., Lehigh University.
- MOSER, R. D. 1989 Statistical analysis of near-wall structures in turbulent channel flow. *Proc. Zoric Intl Seminar on Wall Turbulence* (ed. S. J. Kline). Hemisphere.
- NYCHAS, S. G., HERSHEY, H. C. & BRODKEY, R. S. 1973 A visual study of turbulent shear flow. *J. Fluid Mech.* **61**, 513.
- OFFEN, G. R. & KLINE, S. J. 1974 Combined dye-streak and hydrogen-bubble visual observations of a turbulent boundary layer. *J. Fluid Mech.* **62**, 223.
- OFFEN, G. R. & KLINE, S. J. 1975 A proposed model of the bursting process in turbulent boundary layers. *J. Fluid Mech.* **70**, 209.
- PERRY, A. E. & CHONG, M. S. 1982 On the mechanism of wall turbulence. *J. Fluid Mech.* **119**, 173.
- PURTELL, L. P., KLEBANOFF, P. S. & BUCKLEY, F. T. 1981 Turbulent boundary layer at low Reynolds number. *Phys. Fluids* **24**, 802.
- ROBINSON, S. K., KLINE, S. J. & SPALART, P. R. 1989 Quasi-coherent structures in the turbulent boundary layer: Part II. Verification and new information from a numerically simulated flat-plate layer. *Proc. Zoric Intl Seminar on Wall Turbulence* (ed. S. J. Kline). Hemisphere.
- SCHLICHTING, H. 1979 *Boundary Layer Theory*. McGraw-Hill.
- SCHRAUB, F. A., KLINE, S. J., HENRY, J., RUNSTADLER, P. W. & LITTELL, A. 1965. Use of hydrogen bubbles for quantitative determination of time-dependent velocity fields in low-speed water flows. *Trans. ASME J. Basic Engng* **87**, 429.
- SMITH, C. R. & LU, L. J. 1989 The use of a template-matching technique to identify hairpin vortex flow structures in turbulent boundary layers. *Proc. Zoric Intl Seminar on Wall Turbulence* (ed. S. J. Kline). Hemisphere.
- SMITH, C. R. & PAXSON, R. D. 1983 A technique for evaluation of three-dimensional behavior in turbulent boundary layers using computer augmented hydrogen bubble-wire flow visualization. *Exps. Fluids* **1**, 43.
- SMITH, C. R., WALKER, J. D. A., HAIDARI, A. H. & TAYLOR, B. K. 1990 Hairpin vortices in turbulent boundary layers: the implications for reducing surface drag. In *Proc. IUTAM Symp. on Structure of Turbulence and Drag Reduction* (ed. A. Gyr), pp. 51–58. Springer.
- SPALART, P. R. 1988 Direct simulation of a turbulent boundary layer up to $R_\theta = 1410$. *J. Fluid Mech.* **187**, 61.
- TIEDERMAN, W. G. 1989 Eulerian detection of turbulent bursts. In *Proc. Zoric Intl Seminar on Wall Turbulence* (ed. S. J. Kline). Hemisphere.
- WALKER, J. D. A. 1990 Wall layer eruptions in turbulent flows. In *Proc IUTAM Symp. on Structure of Turbulence and Drag Reduction* (ed. A. Gyr), pp. 101–112. Springer.
- WALLACE, J. M., BRODKEY, R. S. & ECKELMANN, H. 1977 Pattern-recognized structures in bounded turbulent shear flows. *J. Fluid Mech.* **83**, 673.
- WHITE, F. M. 1974 *Viscous Fluid Flow*. McGraw-Hill.